

REGULATORY MECHANISMS OF THE MICRORNA PATHWAY

APPROVED BY SUPERVISORY COMMITTEE

Joshua Mendell, M.D., Ph.D.

Carole Mendelson, Ph.D.

David Russell, Ph. D.

Qinghua Liu, Ph.D.

ACKNOWLEDGMENTS

I have many individuals to thank for their support over the course of this project and during my years prior to pursuing an advanced degree in science. Completing the work presented here would not have been possible without the steady support of my research mentor, Dr. Joshua Mendell, and the many people who I had the fortune to work with in his lab. I was afforded the opportunity to work on the questions that interested me most and given the chance to share my thoughts often and freely with Dr. Mendell. His infectious enthusiasm for finding answers to meaningful questions is something that made our meetings and informal chats one of the most enriching experiences of the lab.

Similarly, I was fortunate to work with curious, motivated lab members every day. The culture of the lab enables anyone to seek out the advice and wisdom of any other member when needed. I want to thank Dr. Antony Hsieh and Dr. Yangjian Liu for guiding my early experiments. My conceptual understanding of this project benefitted significantly from many hours of discussion with Hema Manjunath, Dr. Guanglu Shi, Ryan Hunter, and Dr. Juliane Braun. I especially want to thank Tsung-Cheng Chang for advice and assistance with performing some experiments.

Our collaborators enabled rapid progress on several parts of the CRISPR-Cas9 screening and Argonaute phosphorylation studies. Dr. Yang Xie and Dr. Beibei Chen made critical contributions to the bioinformatics presented here. I am thankful to Dr. James Chen, Dr. Xiang Chen, Dr. Tuo Li, and Dr. Jiayi Wu for advice and for performing the mass spectrometry analysis. I want to thank Dr. Vincent Tagliabracci for his

guidance in studying AGO2 phosphorylation through *in vitro* kinase assays. Dr. Vanessa Schmid, Rachel Bruce, and Ashley Guzman at the Next Generation Sequencing Core of the McDermott Center performed the deep sequencing analysis of this project. Dr. Chao Xing and Mohammed Kanchwala provided technical assistance in analyzing the deep sequencing data. Dr. Haydn Ball and the UT Southwestern Protein Chemistry Technology Core provided assistance through peptide synthesis. Dr. Angela Mobley and the members of the UT Southwestern Flow Cytometry Core performed the FACS analysis for each genome-wide screen. I also wish to thank Stephen Johnson for assistance with software implementation and Jose Cabrera for assistance in preparing figures.

Dr. David Russell, Dr. Carole Mendelson, and Dr. Qinghua Liu all provided guidance and advice as members of my thesis committee. I thank them for their time and thoughtful remarks. The Integrative Biology (IB) program and the UT Southwestern MSTP were also pillars of support during my thesis work.

Many scientists supported my training during my undergraduate years. I am thankful to Dr. Michael Horst, my research mentor of three years at Mercer University. I also want to thank Dr. Roger Miesfeld at the University of Arizona and Dr. J. Troy Littleton at the Massachusetts Institute of Technology for accepting me as a summer student.

Without my family's support, I would undoubtedly not have progressed this far. I am very grateful for their love and attention. They patiently taught me the value of an education and the importance of supporting the needs of others. I still look forward to learning much from them.

REGULATORY MECHANISMS OF THE MICRORNA PATHWAY

BY

RYAN JOSHUA GOLDEN

DISSERTATION

Presented to the Faculty of the Graduate School of Biomedical Sciences
The University of Texas Southwestern Medical Center at Dallas
In Partial Fulfillment of the Requirements
For the Degree of

DOCTOR OF PHILOSOPHY

The University of Texas Southwestern Medical Center
Dallas, Texas
May, 2018

Copyright

by

RYAN JOSHUA GOLDEN, 2016

All Rights Reserved

REGULATORY MECHANISMS OF THE MICRORNA PATHWAY

RYAN JOSHUA GOLDEN, Ph.D.

The University of Texas Southwestern Medical Center at Dallas, 2016

Joshua Mendell, M.D., Ph.D.

MicroRNAs (miRNAs) associate with members of the Argonaute protein family and downregulate partially complementary messenger RNAs (mRNAs) (1). miRNA activity is tightly regulated during development and in normal physiologic settings, while gain or loss of these control mechanisms can contribute to disease (2-4). To identify new mechanisms that regulate the miRNA pathway, we employed CRISPR-Cas9 genome-wide loss-of-function screening (5, 6) coupled with a fluorescent miRNA pathway reporter. These experiments revealed an unanticipated role for the ANKRD52-PPP6C serine/threonine phosphatase complex as a critical regulator of miRNA activity in human cells. Loss of this complex significantly impaired global miRNA

function. Genetic and biochemical studies revealed that phosphorylation of Argonaute2 (AGO2) on a set of highly conserved serine residues, S824-S834, blocks target mRNA engagement. Constitutive activity of the ANKRD52-PPP6C complex is necessary to remove these inhibitory phosphates and thereby allow miRNA-mediated silencing. A genome-wide CRISPR-Cas9 suppressor screen performed in *ANKRD52*^{-/-} cells identified CSNK1A1 as the inhibitory AGO2 kinase that phosphorylates these sites. Together, these findings reveal a previously uncharacterized AGO2 phosphorylation cycle, uncovering a major mechanism through which the miRNA pathway is regulated and highlighting the power of iterative CRISPR-Cas9 screening for the dissection of biological pathways directly in human cells.

TABLE OF CONTENTS

PUBLICATIONS	x
LIST OF FIGURES	xi
LIST OF TABLES	xiii
LIST OF ABBREVIATIONS	xiv
CHAPTER ONE: INTRODUCTION AND REVIEW OF LITERATURE	1
<i>Nucleic acids are essential for life</i>	1
<i>The discovery of microRNAs (miRNAs)</i>	1
<i>The biogenesis of miRNAs</i>	2
<i>The mechanisms of miRNA function</i>	3
<i>Diverse functions of mammalian miRNAs</i>	4
<i>Oncogenesis and the miRNA pathway</i>	4
<i>Regulatory mechanisms of the miRNA pathway</i>	5
<i>Identifying novel regulatory mechanisms of the miRNA pathway</i>	7
<i>Alternative genome-scale screening approaches</i>	8
<i>Projected goals</i>	8
CHAPTER TWO: AN ARGONAUTE REGULATORY PHOSPHORYLATION CYCLE REVEALED BY ITERATIVE CRISPR-CAS9 SCREENING	10
<i>Introduction</i>	10
<i>Results</i>	11
<i>Discussion</i>	56
CHAPTER THREE: DISCUSSION	58
<i>Review of findings</i>	58
<i>Novel transcriptional regulators of the miR-17-92 cluster</i>	58
<i>A novel phosphorylation cycle for AGO2</i>	61
<i>Adapting fluorescent reporters and CRISPR-Cas9 screening to dissect other pathways</i>	66
<i>Summary</i>	66
CHAPTER FOUR: METHODS	68

<i>Construction of miR-19 reporter</i>	68
<i>Generation of HCT116 reporter cell lines</i>	68
<i>Generation of knockout cell lines using CRISPR-Cas9</i>	69
<i>Transfection with miR-19 inhibitors</i>	70
<i>Genome-wide CRISPR-Cas9 screening</i>	70
<i>qRT-PCR</i>	75
<i>RNA-seq</i>	75
<i>Co-immunoprecipitation assays</i>	76
<i>Western blot antibodies</i>	76
<i>Phos-tag SDS-PAGE electrophoresis</i>	77
<i>Mass spectrometry</i>	77
<i>Cloning, mutagenesis, and expression of cDNA constructs</i>	79
<i>AGO2:miRNA and AGO2:mRNA association studies</i>	80
<i>AGO2 capture using an mRNA target mimic</i>	82
<i>Tethering assays</i>	83
<i>Rapamycin treatment of reporter cells</i>	83
<i>In vitro kinase assays using immunopurified FLAG-HA-AGO2</i>	83
<i>In vitro kinase assays using AGO2 peptides</i>	84
APPENDIX	86
BIBLIOGRAPHY	123

PUBLICATIONS

A. N. Walker, **R. Golden**, M. N. Horst, Morphologic effects of in vivo acute exposure to the pesticide methoprene on the hepatopancreas of a non-target organism, *Homarus americanus*. *Ecotoxicol Environ Saf* 73, 1867-1874 (2010).

LIST OF FIGURES

Figure 1: Design of a CRISPR-Cas9 screen to identify regulators of the miRNA pathway.....	12
Figure 2: miR-19 reporter cell lines respond to perturbations of the miRNA pathway....	15
Figure 3: Multiple known and novel regulators revealed in the HCT116 ^{EGFP-miR-19} screen.	16
Figure 4: RIGER analysis reveals lack of enrichment for screen hits from the HCT116 ^{EGFP-miR-19} screen.	17
Figure 5: Knockout of candidate miRNA regulators in HCT116 ^{EGFP-miR-19} cells.	18
Figure 6: Knockout of candidate miRNA regulators in HCT116 ^{EGFP} cells.....	19
Figure 7: Hypothesized scheme of regulation for three transcription-associated genes.	20
Figure 8: Clonal knockouts of BRD4, CTNNB1, and POU2F1 were generated.	21
Figure 9: <i>BRD4</i> , <i>CTNNB1</i> , and <i>POU2F1</i> positively regulate miR-19 biogenesis.....	22
Figure 10: Western blot analysis confirms loss of AGO2 expression.....	23
Figure 11: Western blot analysis confirms loss of ANKRD52 expression.	24
Figure 12: Loss of <i>ANKRD52</i> impairs miRNA-mediated silencing.....	25
Figure 13: Loss of <i>ANKRD52</i> does not impair miRNA biogenesis.	26
Figure 14: FLAG-HA-AGO2 interacts with V5-ANKRD52 and V5-PPP6C.....	27
Figure 15: Loss of either ANKRD52 or PPP6C increases steady-state levels of phosphorylated AGO2.....	28
Figure 16: Sensitivity of AGO2 phosphorylation to lambda protein phosphatase (λ PP).29	
Figure 17: Loss of either ANKRD52 or PPP6C enhances AGO2 phosphorylation in multiple cell lines.	30
Figure 18: FLAG-HA-AGO1 phosphorylation is enhanced in <i>ANKRD52</i> ^{-/-} cells.....	31
Figure 19: Mass spectrometry reveals enhanced phosphorylation of AGO2 at S824-S834.	33
Figure 20: Evolutionary conservation of AGO2 S824-S834.....	34
Figure 21: Identification of multiple definitively phosphorylated residues in the S824-S834 region of AGO2 by mass spectrometry.....	35
Figure 22: AGO2 phosphorylation is abolished by either an S828A mutation or a 5xA mutation.	36

Figure 23: AGO2 phosphorylation impairs mRNA target association but spares miRNA association.	39
Figure 24: AGO2 can be captured from cell lysates using a bait target oligonucleotide.40	
Figure 25: An mRNA target mimic selectively captures non-phosphorylated AGO2.....	41
Figure 26: Phosphomimetic mutants of FH-AGO2 do not exhibit reduced miRNA association.	42
Figure 27: Phosphomimetic mutants of FH-AGO2 exhibit reduced mRNA association. 43	
Figure 28: A phosphomimetic mutant of AGO2 is competent to silence mRNA targets when directly tethered.	44
Figure 29: Design of a CRISPR-Cas9 screen to identify suppressors of the <i>ANKRD52</i> ^{-/-} phenotype.....	47
Figure 30: Four serine/threonine kinases emerge as hits from a genome-wide CRISPR-Cas9 suppressor screen.	48
Figure 31: Analysis of three serine/threonine kinases identified in the CRISPR-Cas9 suppressor screen.....	49
Figure 32: Characterization of <i>ANKRD52</i> ^{-/-} ; <i>CSNK1A1</i> ^{-/-} cells.....	50
Figure 33: A CRISPR-Cas9 suppressor screen reveals CSNK1A1 as the inhibitory AGO2 kinase.....	51
Figure 34: Characterization of miR-19 expression in <i>ANKRD52</i> ^{-/-} ; <i>CSNK1A1</i> ^{-/-} cells. .	52
Figure 35: AGO2 and CSNK1A1 interact in an RNA-independent manner.	53
Figure 36: AGO2 is a direct substrate of CSNK1A1.....	54
Figure 37: An AGO2 phosphorylation cycle regulates target mRNA engagement.	55

LIST OF TABLES

Table 1: Simulated sgRNA enrichment in the top 0.5% brightest cells.	86
Table 2: Top 50 genes by RIGER analysis of CRISPR-Cas9 screen in HCT116 ^{EGFP-miR19} cells.	87
Table 3: Top 50 genes by RIGER analysis of CRISPR-Cas9 screen in HCT116 ^{EGFP} cells.	92
Table 4: Top 50 genes by RIGER analysis of CRISPR-Cas9 screen in <i>ANKRD52</i> ^{-/-} HCT116 ^{EGFP-miR19} cells.	95
Table 5: Oligonucleotide and peptide sequences.	98

LIST OF ABBREVIATIONS

AGC	Automatic gain control
ATP	Adenosine triphosphate
Autorad	Autoradiograph
BSA	Bovine serum albumin
Cas9	CRISPR associated protein 9
CK1	Casein kinase 1
Co-IP	Co-immunoprecipitation
CRISPR	Clustered regularly interspaced short palindromic repeats
DNA	Deoxyribonucleic acid
DTT	Dithiothreitol
EDTA	Ethylenediaminetetraacetic acid
EGFP	Enhanced green fluorescent protein
EGTA	Ethylene Glycol Tetraacetic Acid
FACS	Fluorescence-activated cell sorting
FDR	False discovery rate
GFP	Green fluorescent protein
HCD	Higher-energy collisional dissociation
IP	Immunoprecipitation
LC	Liquid chromatography
λ N	Lambda N
lncRNA	Long non-coding RNA
λ PP	Lambda protein phosphatase
miRNA	microRNA
MOI	Multiplicity of infection
MS	Mass spectrometry
MSCV	Murine stem cell virus
ND	Not detected
NES	Normalized enrichment score
ORF	Open reading frame
PAGE	Polyacrylamide gel electrophoresis
p-AGO2	Phospho-AGO2
PBS	Phosphate buffered saline
PCR	Polymerase chain reaction
pri-miR-17-92	Primary microRNA-17-92 transcript
qRT-PCR	Quantitative reverse transcription-polymerase chain reaction
RIGER	RNAi gene enrichment ranking
RNA	Ribonucleic acid
RNAi	RNA interference
RNA-seq	RNA sequencing

SA	Specific activity
SBR	Second best rank
SD	Standard deviation
SDS	Sodium dodecyl sulfate
SFCA	Surfactant-free cellulose acetate
sgRNA	Single guide RNA
shRNA	Small hairpin RNA
snRNA	Small nuclear RNA
TE	Tris, EDTA
UT	University of Texas
UTR	Untranslated region
WT	Wild type

CHAPTER ONE

Introduction and Review of Literature

Nucleic acids are essential for life

Living organisms depend upon the production of protein through elaborate molecular processes first initiated by transcription of deoxyribonucleic acid (DNA) into ribonucleic acid (RNA) (7). The process of translation employs the ribosome to produce protein by directly reading the protein sequence information embedded within the messenger RNA (mRNA) strand. Curiously, not all RNA strands code for protein sequences. RNAs that do not code for protein sequences, non-coding RNAs, can participate in a range of functions involved in cellular homeostasis (8). Their numbers are vast, and the roles they serve are being elucidated at a growing pace.

Early work demonstrated a critical role for non-coding RNAs in driving the process of translation. Transfer RNAs (tRNAs) and ribosomal RNAs (rRNAs) are two such species that were identified as key components of the molecular machinery for this event (9). Later work identified a class of RNAs involved in the regulation of splicing, the process by which large sequences of RNA are precisely resected from a precursor mRNA (pre-mRNA) (10). More recent studies have established a role for an additional class of non-coding RNAs, long non-coding RNAs (lncRNAs), in governing complex processes such as chromatin remodeling and transcription (11).

The discovery of microRNAs (miRNAs)

Studies of heterochronic genes in *C. elegans* yielded the surprising discovery that small RNAs of only ≈ 22 nucleotides in length are capable of repressing mRNAs sharing partial complementarity (12-14). These foundational studies prompted a race to characterize the mechanisms by which these small RNAs function and the extent to which they are present across various organisms. Further studies determined that this type of small RNA includes hundreds of members and exists across multiple phyla (15-17). The term microRNA (miRNA) was coined to identify this class of small RNAs. Several key observations were made at this point. Not only are miRNAs present across multiple phyla, many miRNAs were determined to be conserved across phyla. The expression pattern for miRNAs was studied and found to vary in some cases based on the tissue or point in organismal development. Not only was miRNA expression correlated with development, studies also revealed that particular miRNAs, such as *lin-4* in *C. elegans*, are required for proper development. Together, these studies identified a novel, abundant class of RNA that regulates gene expression at the post-transcriptional level.

The biogenesis of miRNAs

Ambros and colleagues observed two small RNA species when examining the RNA products from *lin-4* (12). They correctly hypothesized that the larger product of approximately 60 nt, *lin-4L*, was processed into the smaller form, *lin-4S*. Many years would pass before the literature finally confirmed this assertion. The RNase III enzyme Dicer was discovered to cleave small RNA hairpins, known as precursor miRNAs (pre-miRNAs), and promote the formation of the final mature miRNA duplex (18, 19). The origins of the pre-miRNA species were found to result from nuclear processing of longer

primary miRNA transcripts, pri-miRNAs (20). Kim and colleagues went on to identify the RNase III family member Drosha as the primary nuclease for cleaving pri-miRNAs into pre-miRNA hairpins (21). Mature miRNA sequences of approximately 22 nucleotides in length are bound by members of the Argonaute protein family, and these proteins mediate the functions of miRNAs (19, 22). The mature complex of a miRNA and Argonaute protein is formed as a pre-miRNA is processed by Dicer, and the resulting duplex is loaded into Argonaute where a single, functional miRNA strand is retained (23).

The mechanisms of miRNA function

The first reports of miRNAs appreciated the existence of sequence complementarity between a miRNA and a given mRNA target (12, 13). The discovery that Argonaute proteins mediate the functions of miRNAs led to a series of reports documenting various mechanisms by which AGO-miRNA complexes are able to silence targeted transcripts. Ambros and colleagues noted that despite the ability of *lin-4* to reduce the protein levels of LIN-14, the levels of the *lin-14* mRNA were unchanged (12). This observation strongly supported a role for miRNAs in suppressing translation of a targeted mRNA but not necessarily reducing mRNA levels. Many later reports supported a role for miRNAs in impairing translation, specifically at the initiation step, of targeted transcripts (24-26). In contrast, more comprehensive studies looking at the global transcriptome supported a role for miRNAs in reducing mRNA levels as well (27, 28). Though miRNAs do appear to function in part through translational repression, the dominant mechanism by which they function for most targets involves triggering transcript decay (29-32). Curiously, a later assessment of *lin-14* mRNA levels

confirmed that lin-4 also suppresses LIN-14 protein expression by triggering transcript decay (33).

Diverse functions of mammalian miRNAs

To date, hundreds of mammalian miRNAs have been identified (34, 35). Given that most mRNAs are conserved targets for miRNA regulation, a vast network of potential functions for miRNAs exists (36). Animal knockout experiments have been fruitful for demonstrating the *in vivo* roles for individual miRNAs and miRNA families in mammalian physiology and disease. Loss of a central component of miRNA biogenesis, *Dicer1*, results in embryonic lethality in mice (37). Hemizygous loss of a conserved cluster of miRNAs, the miR-17-92 cluster, in mice and humans results in skeletal abnormalities (38). Homozygous loss of the cluster in mice results in impaired lung, heart, and B cell development (39). Loss of miR-138 in mice promotes enhanced motor activity and drives lethal epilepsy (40). Deletion of the miR-290-295 cluster facilitates partially penetrant lethality in mutant embryos and leads to germ cell defects in surviving animals (41). In some cases, deletion of a miRNA or miRNA cluster does not yield an overt phenotype unless the animal undergoes some period of stress. For example, loss of the miR-143/145 cluster yields no obvious phenotype in mouse development or baseline homeostasis (42). However, these animals exhibit a profound deficit in tissue regeneration following the stress of chemically-induced colitis. In sum, these reports illustrate a few of the many *in vivo* studies that have established a biologically significant role for miRNAs in governing cellular homeostasis.

Oncogenesis and the miRNA pathway

MicroRNA dysregulation has been documented in numerous disease states using human tissue samples as well as with complementary animal models (4). In no area has this perhaps been more rigorously investigated than in oncogenesis. Within mouse models, overexpression of select miRNAs has been demonstrated to drive lymphomagenesis (43, 44). Enforced expression of either miR-155 or miR-21 is capable of promoting B cell lymphoma in mice. Similarly, overexpression of a portion of the miR-17-92 cluster cooperates with Myc-driven oncogenic programs to drive lymphomagenesis in mice (45). Later studies highlighted the role of a single pair of miRNAs, miR-19a and miR-19b, in driving Myc-induced lymphomagenesis (46, 47). In contrast, therapeutic delivery of miRNAs with proposed tumor suppressor functions has been demonstrated to impair oncogenic progression in genetic murine models of cancer. For example, systemic delivery of miR-26 by an adeno-associated virus impedes tumor progression of a murine model of liver cancer (48).

Regulatory mechanisms of the miRNA pathway

The regulation of the miRNA pathway has been the subject of intense scrutiny since the initial discovery of miRNAs. Given the consequences of dysregulation of the pathway, it is no surprise that a plethora of regulatory points have emerged to govern miRNA activity (2). Many of these mechanisms rely upon controlling the production or turnover of individual miRNAs or a bulk population of miRNAs. Transcriptional regulation is commonly employed to produce a given miRNA or miRNA family when needed. The pro-growth pri-miR-17-92 cluster is transcribed in response to transactivation by Myc, a mechanism commonly exploited in lymphomagenesis (49). Levels of miR-16 family members are known to fluctuate throughout the cell cycle, and

this regulation was determined to be at the level of transcription (50). Some miRNA members respond to circadian transcriptional programs, as seen through the ability of REV-ERB α to regulate the pri-miR-122 transcription (51). Systematic mapping of hundreds of primary miRNA transcripts in mouse and human cells has provided a useful tool for those wishing to characterize potential transcriptional regulatory events in the miRNA pathway (52). Undoubtedly, this particular node of regulation will continue to be characterized for the hundreds of annotated miRNAs.

Post-transcriptional regulation of miRNA production is another reported mechanism to regulate miRNA activity. One extensively studied example of this phenomenon involves impaired production of mature let-7 from its precursor forms (53, 54). Binding of Lin28 to pri-let-7 impairs the ability of DROSHA to process this RNA to the pre-let-7 form, and binding of Lin28 to pre-let-7 promotes turnover of this RNA precursor (55). These mechanisms together act to reduce let-7 levels with significant biological consequences, particularly with respect to accelerating oncogenic progression (56). The activity of DROSHA is subject to regulation by other regulatory factors as well. A non-canonical function of p53 has been documented by which it associates with the DROSHA processing complex and enhances the processing of a subset of miRNAs (57). Additionally, cell confluency has been shown to affect the activity of the DROSHA complex through the Hippo signaling pathway (58). These examples illustrate a few of the mechanisms by which cells exert post-transcriptional control over the miRNA pathway.

The central proteins enabling the functions of miRNAs are adorned by post-translational modifications (59-64). Some of these modifications are triggered by acute

stress and serve to orchestrate a coordinated response by the miRNA pathway. For example, hypoxic conditions promote phosphorylation of AGO2 at Y393, and this event impairs the biogenesis and therefore activity of select miRNAs (63). In other cases, constitutive modification of a miRNA pathway component is necessary for efficient silencing in the absence of acute stress. These events allow the pathway to overcome inherent limitations of the unmodified machinery. An example includes the dependence of Drosha upon phosphorylation for its proper localization (65, 66). Defining the post-translational events that are fundamental for optimal activity of the miRNA pathway remains an open area of inquiry.

Identifying novel regulatory mechanisms of the miRNA pathway

Characterizing the full complexity of the miRNA pathway is a daunting task, and elucidating the many regulatory mechanisms in place to govern its function remains a fruitful area of research. Interrogating this question does not require a single formulaic approach but can be accomplished through various means. Comprehensive, genome-scale screens for fundamental regulatory mechanisms of miRNA activity have been successfully used in *C. elegans* and *D. melanogaster* (67, 68). Such studies allow one to identify regulatory components necessary for miRNA function under physiological conditions. To my knowledge, no comprehensive genome-scale loss-of-function study has been carried out to identify novel regulatory components of the miRNA pathway directly in human cells. Traditionally, such a screen may have relied upon the use of small interfering RNAs (siRNAs) or small hairpin RNAs (shRNAs) as a platform for silencing genes using RNA interference (RNAi) (69). Unfortunately, the proteins

mediating miRNA and siRNA functions in human cells are shared (70); therefore, an alternative genome-scale screening strategy is required.

Alternative genome-scale screening approaches

Recent advances in genome engineering have provided novel platforms for conducting genome-wide screens. The discovery of a programmable RNA-guided DNA endonuclease system in bacteria [Clustered Regularly Interspaced Short Palindromic Repeats (CRISPR), CRISPR associated protein (Cas9)] provided a multifunctional tool that has been adapted for genetic manipulations in human cells (71-73). Loss-of-function studies using Cas9 have been extended to the genome-scale and successfully used to identify novel regulators of diverse cellular functions (6, 74). Performing a genome-wide loss-of-function screen using CRISPR-Cas9 to uncover novel regulatory mechanisms of the miRNA pathway allows one to escape three key limitations of screens using RNAi. (1) RNAi cannot facilitate a complete genetic loss-of-function, whereas effective CRISPR-Cas9 targeting can ablate gene function (75). (2) Off-target effects plague RNAi studies given that many unintended mRNA targets are subject to regulation by exogenous siRNAs or shRNAs via a mechanism similar to endogenous miRNAs (75). In contrast, careful design of single guide RNAs (sgRNAs), the factors necessary for targeting of Cas9, can offer very stringent specificity (76). (3) The activity of CRISPR-Cas9 is not dependent upon the miRNA pathway, in stark contrast to an RNAi-based screen.

Projected goals

Previous genome-wide screens for regulators of the miRNA pathway have yielded several novel candidate genes (67, 68). For this project, I intend to design a novel screening platform using CRISPR-Cas9 to identify biologically significant regulators of miRNA function directly in human cells. Carrying out the screen under physiological cell culture conditions will allow me to identify novel putative regulators of the pathway, with a strong possibility of identifying factors necessary for miRNA function in the absence of acute stress. Completing this stage of the project will provide a list of novel putative regulators of the pathway. We then plan to validate candidate regulators and rigorously dissect the mechanisms by which several of these genes function. In sum, this project will provide a list of candidate regulators for other groups to dissect further, but more importantly, this project itself will define the mechanisms by which several genes act to regulate miRNA function in humans.

CHAPTER TWO

An Argonaute Regulatory Phosphorylation Cycle Revealed by Iterative CRISPR-Cas9 Screening

Introduction

The miRNA pathway is subject to numerous regulatory mechanisms under physiological growth conditions and in response to acute stress (2). To identify novel regulatory components of the pathway, a fluorescent reporter could be established to provide a readout of miRNA activity in living cells. Coupling fluorescence activated cell sorting (FACS) analysis and an established CRISPR-Cas9 loss-of-function screening system (6, 77) would allow one to utilize a fluorescent reporter of miRNA activity and search for novel regulators. An existing miRNA target sequence (78) could be adapted for use with Green Fluorescence Protein (GFP) to generate such a reporter.

A key question in designing the reporter involves determining which individual miRNA will serve as a suitable representative miRNA. Ideally, such a miRNA would be abundantly expressed across multiple cell lines and have an established biological significance, should any findings be specific to just that miRNA. The miR-17-92 cluster contains two miRNAs, miR-19a and miR-19b, whose expression drives Myc-driven lymphomagenesis in mice (46, 47, 79). miR-19a and miR-19b, collectively referred to as miR-19, are abundantly expressed in the stably diploid colon cancer cell line, HCT116 (80). Additionally, previous studies have demonstrated successful genome-scale screening using this cell line (81), making it a strong candidate cell line for further comprehensive genome-wide loss-of-function screens.

In this study, a fluorescent reporter was generated to detect miR-19 activity in human cells. A genome-scale loss-of-function screen was performed using an established CRISPR-Cas9 library targeting over 19,000 protein-coding genes and over 1,000 annotated miRNAs in humans (5, 6). Hits from the screen were scored for statistical significance, and many of the strongest hits were subjected to further mechanism-based studies. These subsequent experiments revealed a novel transcriptional network underlying the biogenesis of miR-19. They also revealed a novel phosphoregulatory cycle that can uncouple Argonaute's ability to bind miRNAs and mRNA targets.

Results

To apply genome-wide CRISPR-Cas9 screening to interrogate the miRNA pathway, we envisioned a strategy wherein a cell line expressing a fluorescent reporter of miRNA activity would be transduced with a pooled library consisting of Cas9 and a repertoire of single guide RNAs targeting most protein-coding genes (6) (Fig. 1). Cells deficient in miRNA activity could then be enriched by fluorescence activated cell sorting. Subsequent determination of sgRNA representation in the sorted versus unsorted cells using high-throughput sequencing would potentially allow the identification of novel core components and regulators of the pathway.

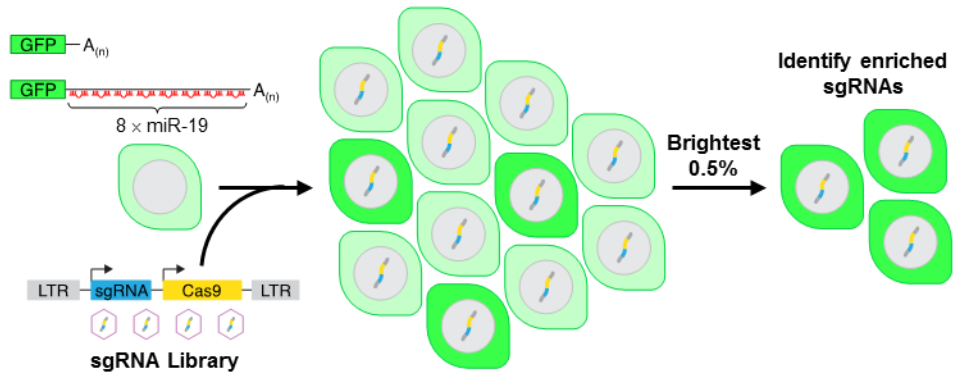


Figure 1: Design of a CRISPR-Cas9 screen to identify regulators of the miRNA pathway.

To implement this strategy, we first generated a reporter cell line that provides a sensitive fluorescent read-out of miRNA activity. An *enhanced green fluorescent protein (EGFP)* transcript with a 3' untranslated region (UTR) embedded with eight imperfectly complementary binding sites for miR-19, an abundant model miRNA, was constitutively expressed in the stably diploid cell line HCT116 (82). Since miR-19 has established oncogenic activity in multiple tumor types (46, 79), we reasoned that specific regulators of this miRNA as well as global regulators of the miRNA pathway would both be of potential interest, should they emerge from the screen. A control cell line with *EGFP* lacking miR-19 binding sites was generated in parallel. To assess the regulation of these reporters, respectively termed HCT116^{EGFP-miR19} and HCT116^{EGFP}, by the miRNA pathway, cells were transduced with lentiviruses expressing Cas9 and either a negative control sgRNA, an sgRNA targeting *EGFP*, or an sgRNA targeting the essential miRNA biogenesis factor *DROSHA* (Fig. 2, top). As expected, *DROSHA* loss of function derepressed EGFP specifically in HCT116^{EGFP-miR19} cells whereas *EGFP*-targeting sgRNAs efficiently silenced EGFP in both lines. Further confirming the regulation of the miRNA reporter by endogenous miR-19, transfection with antisense miR-19 inhibitors strongly enhanced EGFP expression in HCT116^{EGFP-miR19} but not HCT116^{EGFP} cells (Fig. 2, bottom).

Having validated the responsiveness of HCT116^{EGFP-miR19} cells to perturbations of the miRNA pathway, a genome-wide CRISPR-Cas9 screen was carried out by infecting these cells with a pooled lentiviral sgRNA library targeting over 19,000 human genes and 1864 miRNAs (5). After 14 days of growth, cells with relative impairment of the miRNA pathway were enriched by collecting the brightest 0.5% of cells by FACS. This

cut-off was chosen based on simulations demonstrating that collecting cells in this gate could theoretically yield >150-fold enrichment of highly effective sgRNAs that target essential genes in the miRNA pathway (Appendix, Table 1). Moreover, these simulations suggested that even partially effective guides that incompletely impair miRNA-mediated silencing would be strongly enriched. sgRNA representation in the sorted and unsorted cells was enumerated by high-throughput sequencing and the RNAi Gene Enrichment Ranking (RIGER) algorithm was used to identify genes targeted by multiple enriched sgRNAs, representing high-confidence hits (83) (Appendix, Table 2). A parallel screen in HCT116^{EGFP} cells was carried out to identify false positives that directly regulate EGFP expression (Appendix, Table 3). A large number of established core components of the miRNA pathway and miR-19 itself were identified as highly significant hits in HCT116^{EGFP-miR19} but not HCT116^{EGFP} cells (Figures 3-4), establishing the sensitivity of this approach to identify known and potentially novel components of the pathway.

Among the most highly ranked genes without a previously defined role in the miRNA pathway, we noted two classes of potentially novel regulators: genes associated with transcriptional regulation (*BRD4*, *CTNNB1*, and *POU2F1*) and components of the serine/threonine protein phosphatase 6 (PPP6) complex (*ANKRD52* and *PPP6C*). Validation studies confirmed that loss of function of any of these five genes measurably derepressed *EGFP* in HCT116^{EGFP-miR19} but not HCT116^{EGFP} cells (Figures 5-6).

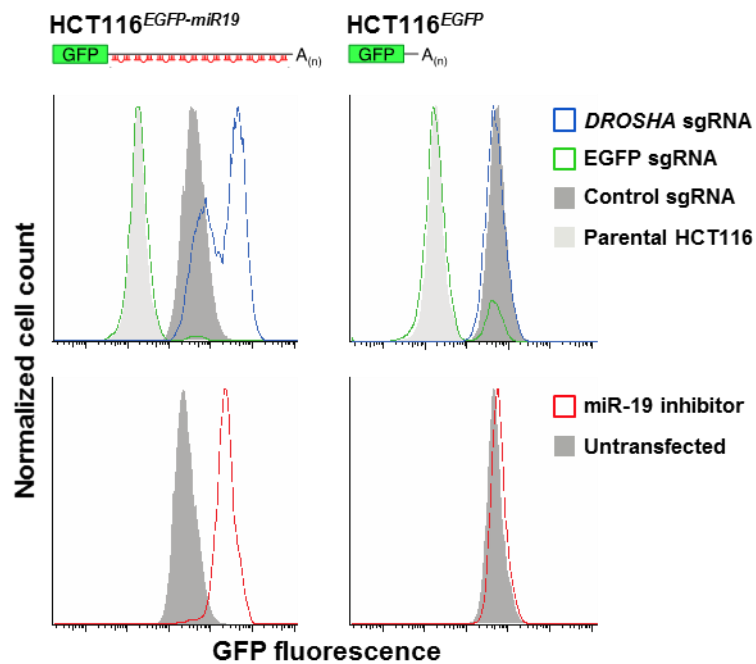


Figure 2: miR-19 reporter cell lines respond to perturbations of the miRNA pathway. Functional validation of the HCT116^{EGFP-miR19} and HCT116^{EGFP} reporter cell lines. EGFP fluorescence was assessed in cells transduced with lentiCRISPR vectors expressing the indicated sgRNAs (top) or after transfection with antisense miR-19 inhibitors (bottom).

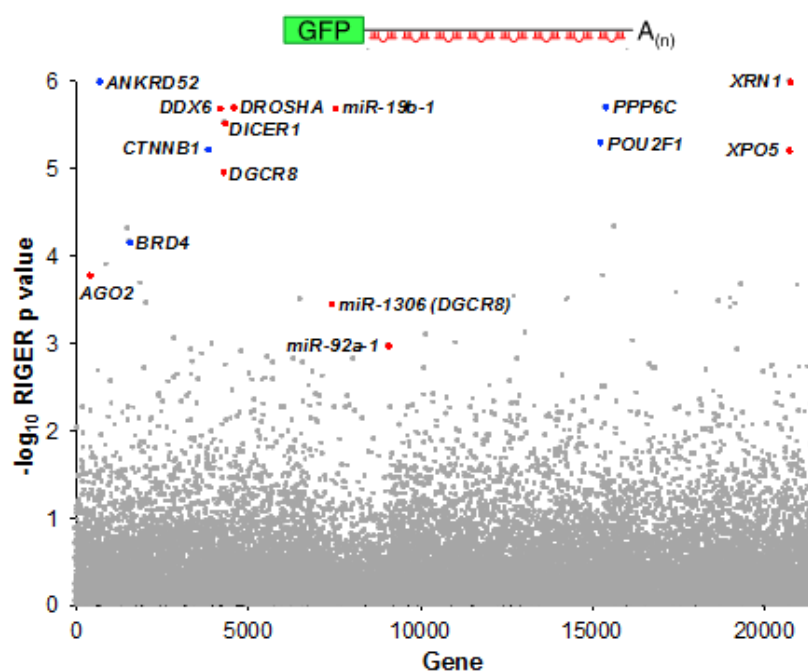


Figure 3: Multiple known and novel regulators revealed in the HCT116^{EGFP-miR-19} screen. RIGER analysis of screening results in HCT116^{EGFP-miR19} cells. Red dots indicate known components of the miRNA pathway while blue dots represent putative novel regulators.

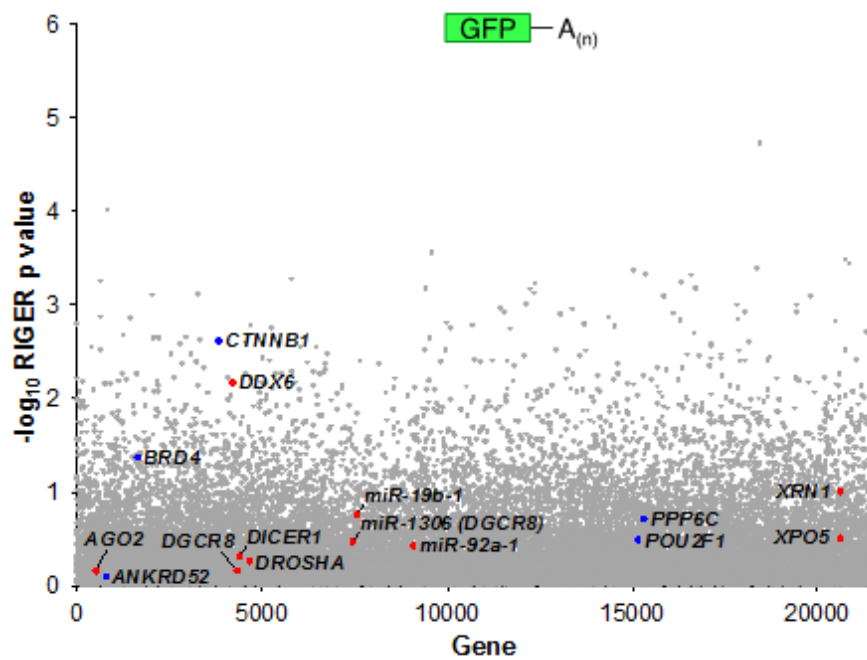


Figure 4: RIGER analysis reveals lack of enrichment for screen hits from the HCT116^{EGFP-miR-19} screen. RIGER analysis of screening results in HCT116^{EGFP} cells. Red dots indicate known components of the miRNA pathway while blue dots represent putative novel regulators.

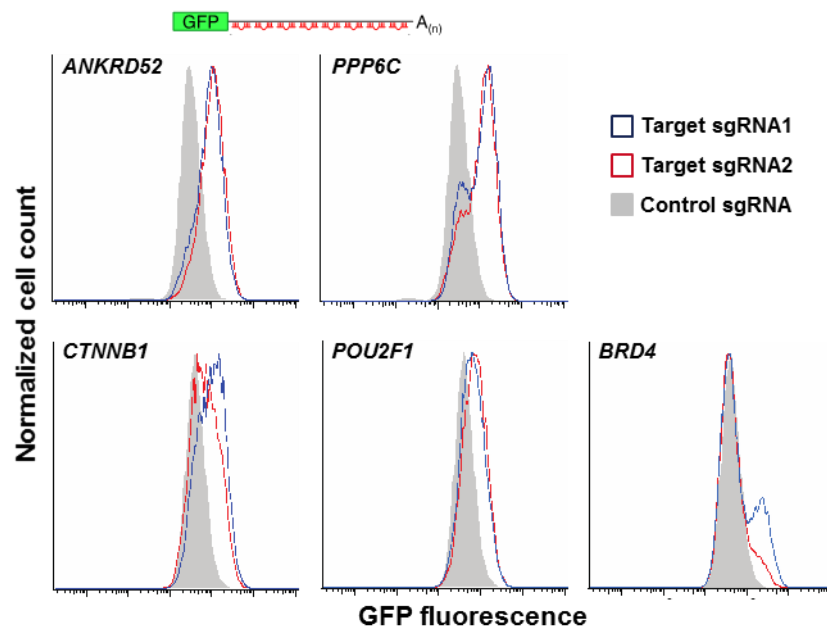


Figure 5: Knockout of candidate miRNA regulators in HCT116^{EGFP-miR-19} cells. Flow cytometry demonstrating derepression of EGFP in HCT116^{EGFP-miR19} cells after transduction with lentiCRISPR vectors targeting the indicated candidate genes.

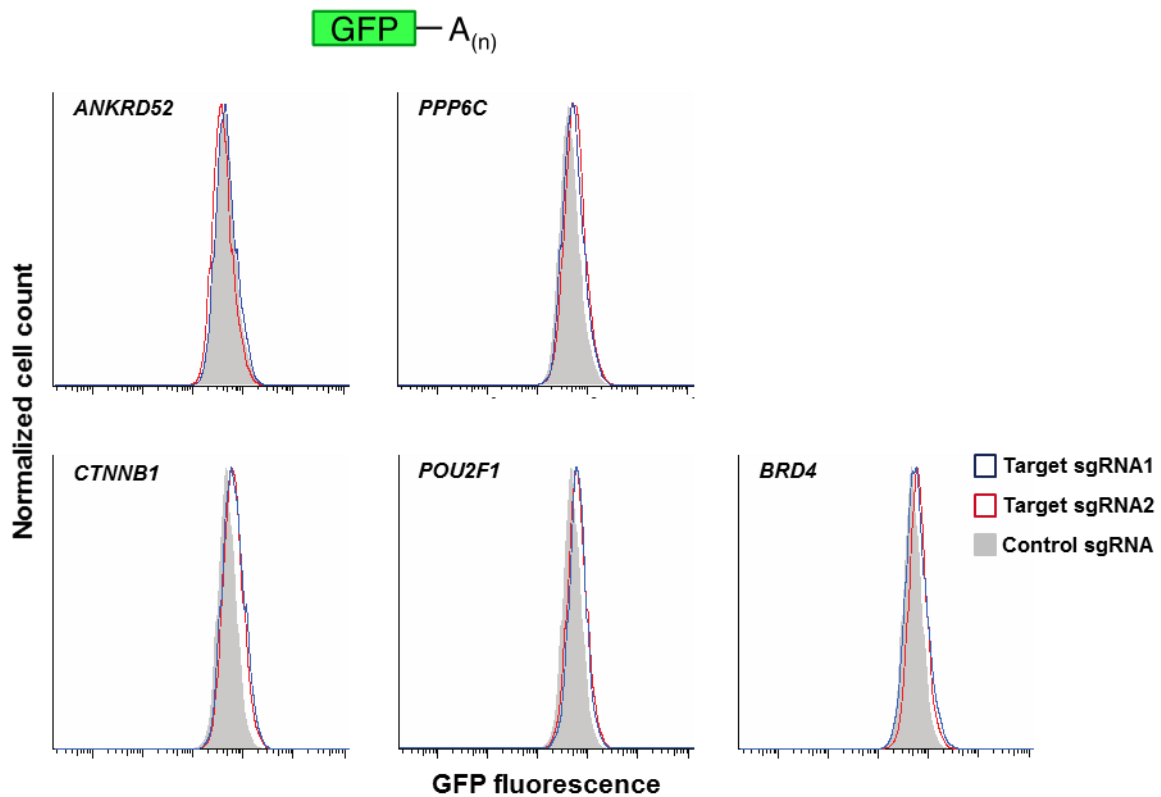


Figure 6: Knockout of candidate miRNA regulators in HCT116^{EGFP} cells. Flow cytometry analysis of EGFP in HCT116^{EGFP} cells after transduction with lentiCRISPR vectors targeting the indicated genes.

Given that *CTNNB1* and *BRD4* promote *MYC* expression (84, 85), a known positive regulator of miR-19 transcription (49), we speculated that these genes indirectly regulate miR-19 expression. In keeping with this hypothesis, clonally-derived *CTNNB1*^{-/-} and *BRD4*^{-/-} cells exhibited reduced expression of *MYC*, reduced expression of the miR-17-92 primary transcript (pri-miR-17-92) which encodes miR-19, and reduced mature miR-19 levels (Figures 7-9). *POU2F1*^{-/-} cells also exhibited reduced pri-miR-17-92 and mature miR-19, but *MYC* expression was unchanged, suggesting that *POU2F1* promotes transcription of pri-miR-17-92 through an alternative mechanism.

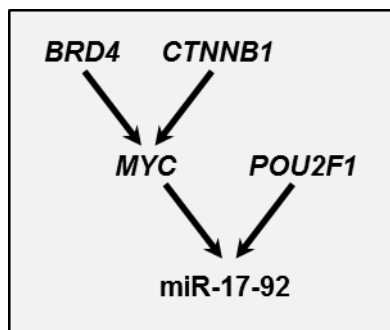


Figure 7: Hypothesized scheme of regulation for three transcription-associated genes. *BRD4* and *CTNNB1* are both known to regulate the transcription of *MYC*. *POU2F1* may directly regulate the transcription of the miR-17-92 cluster.

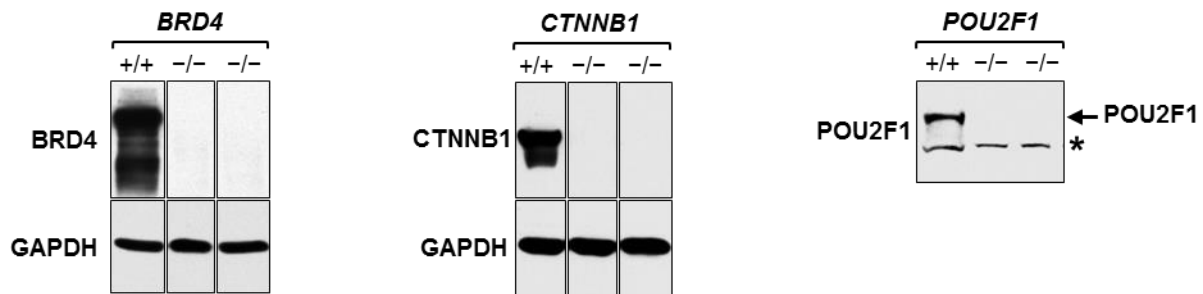


Figure 8: Clonal knockouts of BRD4, CTNNB1, and POU2F1 were generated. Western blot experiments confirm that clonal knockout cell lines were established in HCT116 for three different genes. Two independent clones were derived per cell line. Asterisk indicates a non-specific band.

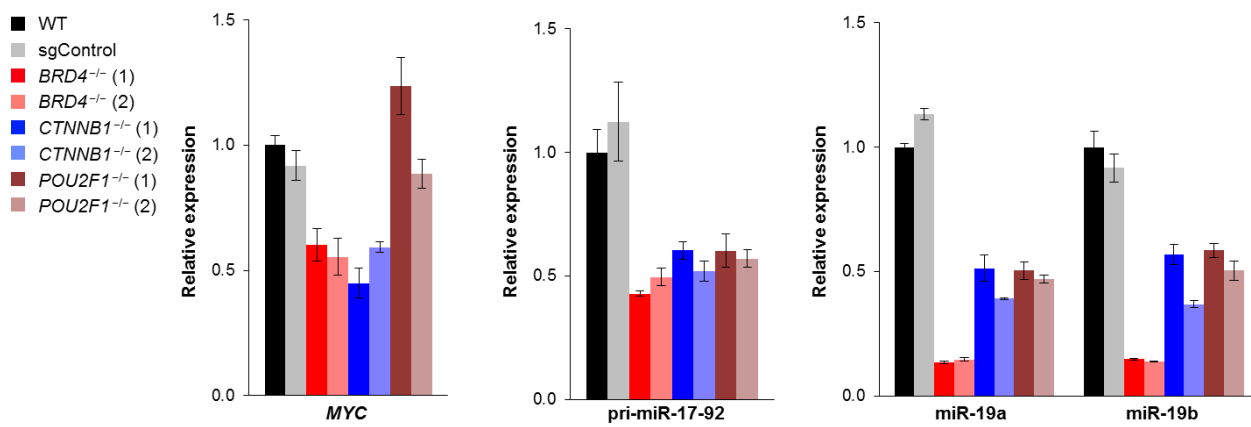


Figure 9: *BRD4*, *CTNNB1*, and *POU2F1* positively regulate miR-19 biogenesis. Quantitative reverse transcription-polymerase chain reaction (qRT-PCR) assays demonstrate reduced MYC expression in cells deficient for either *BRD4* or *CTNNB1*. Loss of either *BRD4*, *CTNNB1*, or *POU2F1* impairs biogenesis of miR-19 and is associated with a reduction in pri-miR-17-92. (Data generated by Tsung-Cheng Chang.)

The identification of ANKRD52 and PPP6C, interacting components of the PPP6 complex (86), as high-scoring hits was of particular interest since it suggested that phosphorylation strongly regulates the activity of an essential miRNA pathway component. Thus, we examined whether loss of ANKRD52 results in a global defect in miRNA-mediated silencing. RNA-seq was performed on cells deficient for Argonaute 2 (AGO2), revealing 431 genes that were significantly upregulated upon loss of this core factor in the miRNA pathway (Figure 10). These genes were similarly upregulated in *ANKRD52*^{-/-} cells (Figures 11 and 12), consistent with a general impairment of miRNA-mediated silencing. Diminished miRNA activity in *ANKRD52*^{-/-} cells was not accompanied by a decrease in the steady-state abundance of a panel of representative miRNAs (Figure 13), indicating that the ANKRD52-PPP6C complex does not measurably regulate miRNA biogenesis.

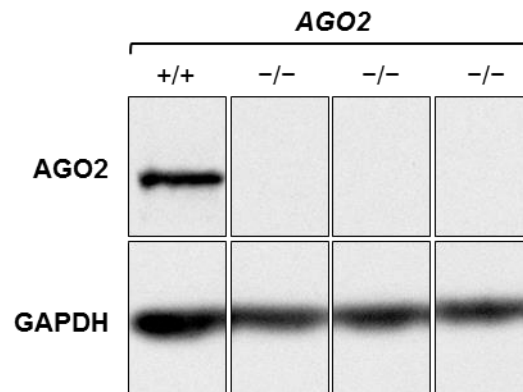


Figure 10: Western blot analysis confirms loss of AGO2 expression. All samples came from the same western blot and irrelevant lanes were removed.

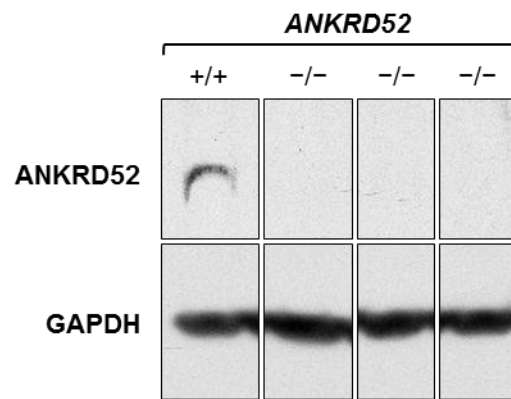


Figure 11: Western blot analysis confirms loss of ANKRD52 expression. All samples came from the same western blot and irrelevant lanes were removed.

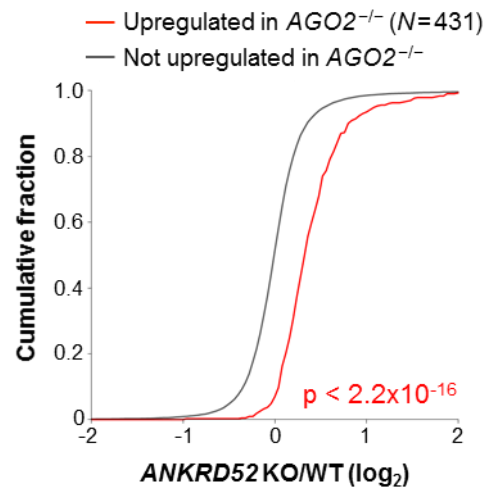


Figure 12: Loss of *ANKRD52* impairs miRNA-mediated silencing. Cumulative distribution plot demonstrating that genes upregulated in *AGO2*^{-/-} HCT116 cells (FDR ≤ 0.05) are similarly upregulated in *ANKRD52*^{-/-} cells (Kolmogorov-Smirnov p value shown).

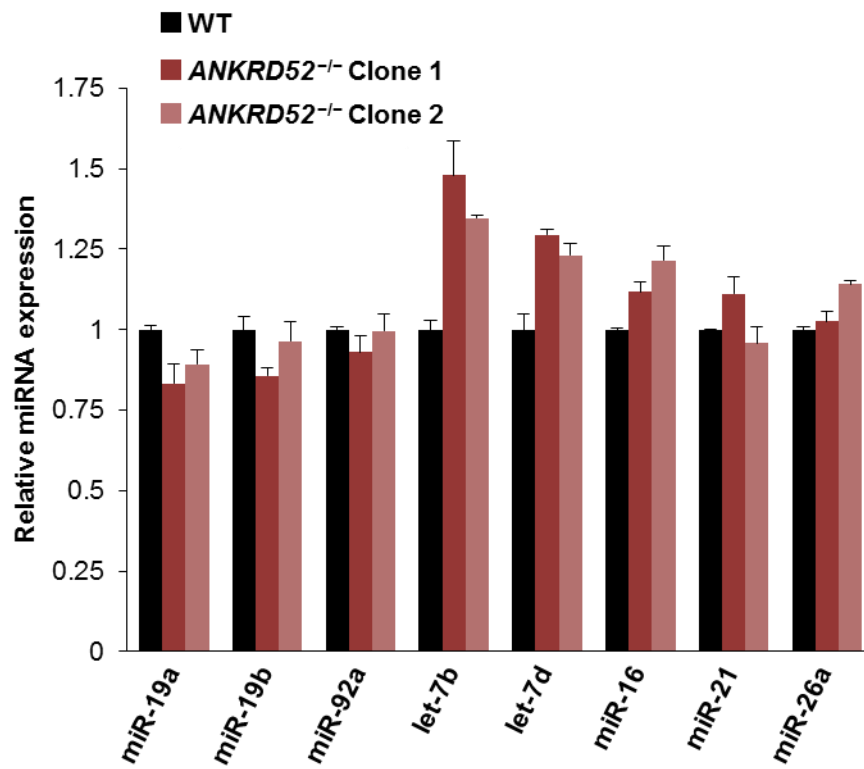


Figure 13: Loss of *ANKRD52* does not impair miRNA biogenesis. qRT-PCR was performed for the indicated miRNAs and expression levels were normalized to U6 snRNA ($N = 2$ biological replicates, each assayed in triplicate).

Since Argonaute proteins are universal effectors of miRNA-mediated silencing, we hypothesized that human Argonautes may be dephosphorylated and activated by ANKRD52-PPP6C. Consistent with this hypothesis, co-immunoprecipitation demonstrated that both ANKRD52 and PPP6C interacted with human AGO2 in an RNA-independent manner (Figure 14). Phos-tag electrophoresis, a sensitive method for detection of phosphorylated proteins (87), revealed that AGO2 migrated as a doublet, with dramatic enhancement of the slowly migrating form in cells deficient for ANKRD52 or PPP6C (Figure 15). Treatment with lambda protein phosphatase collapsed the doublet to a single band (Figure 16), confirming that the slower migrating species corresponds to phosphorylated AGO2 (p-AGO2). Deficiency of ANKRD52 or PPP6C in multiple human cell lines similarly led to accumulation of phosphorylated AGO2 (Figure 17), demonstrating that these observations are not limited to HCT116 cells. We also observed enhanced phosphorylation of AGO1 in *ANKRD52*^{-/-} cells (Figure 18), suggesting broader regulation of Argonaute proteins by the ANKRD52-PPP6C complex.

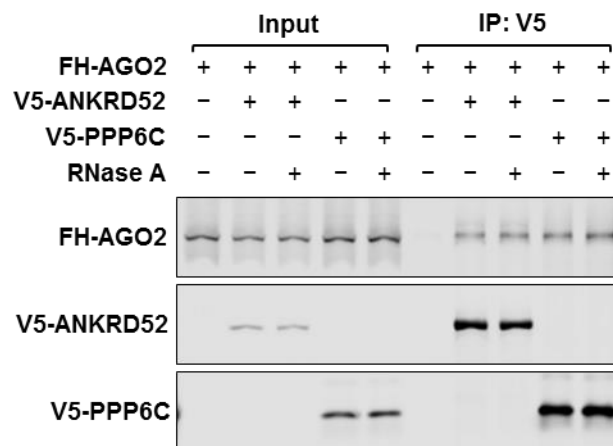


Figure 14: FLAG-HA-AGO2 interacts with V5-ANKRD52 and V5-PPP6C. Co-immunoprecipitation of FLAG-HA-AGO2 (FH-AGO2) with V5-ANKRD52 or V5-PPP6C with or without RNase A treatment.

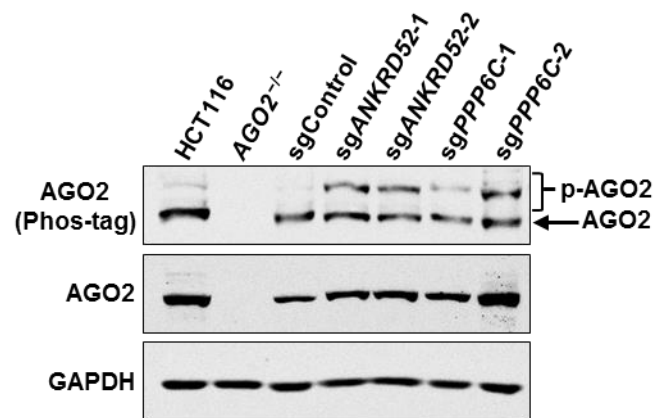


Figure 15: Loss of either ANKRD52 or PPP6C increases steady-state levels of phosphorylated AGO2. Phos-tag electrophoresis demonstrating enhanced AGO2 phosphorylation in ANKRD52/PPP6C-deficient HCT116 cells.

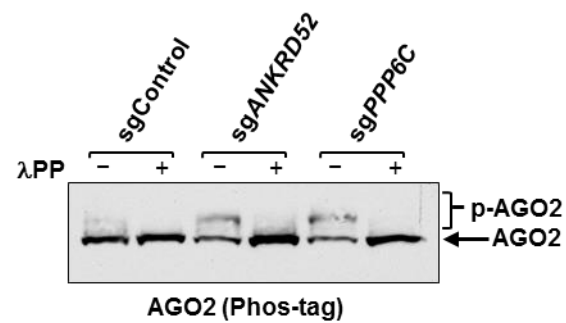


Figure 16: Sensitivity of AGO2 phosphorylation to lambda protein phosphatase (λ PP). Treatment of cell lysates with λ PP collapses the slowly migrating AGO2 band.

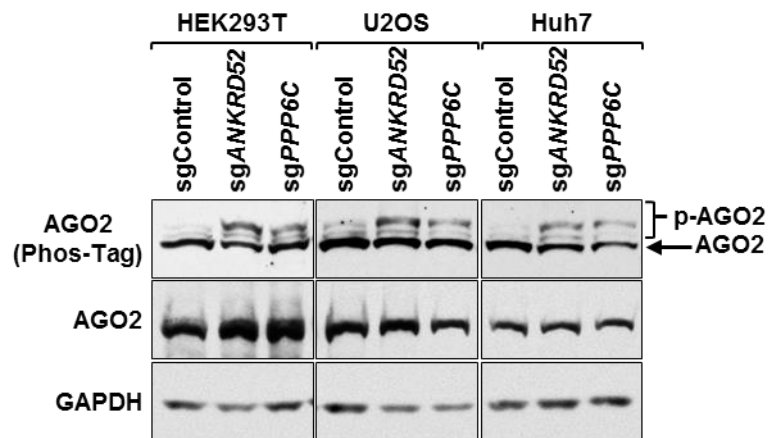


Figure 17: Loss of either ANKRD52 or PPP6C enhances AGO2 phosphorylation in multiple cell lines. Phos-tag western blot analysis of AGO2 in multiple cell lines treating with lentiCRISPR virus targeting either *ANKRD52* or *PPP6C*.

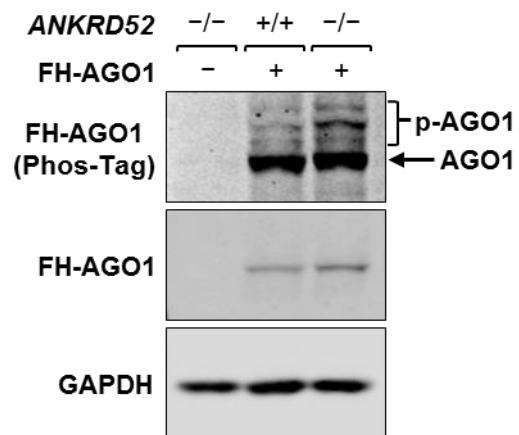


Figure 18: FLAG-HA-AGO1 phosphorylation is enhanced in *ANKRD52*^{-/-} cells. Phos-tag western blot analysis of FLAG-HA-AGO1 (FH-AGO1) stably expressed in *ANKRD52*^{+/+} and *ANKRD52*^{-/-} HCT116 cells.

Mass spectrometry was used to identify the residue(s) in endogenous AGO2 that become hyperphosphorylated in the absence of ANKRD52. Enhanced phosphorylation within a region of the PIWI domain containing four highly conserved serine residues and a single poorly conserved threonine residue (S824-S834) was detected in *ANKRD52*^{-/-} cells, while the previously reported phosphorylation of S387(88) was not increased (Figure 19-21a). Triply phosphorylated peptides spanning S824-S834 were detected, demonstrating phosphorylation of at least three residues in this region, with definitive detection of p-S824 (Figure 21b). Since the large number of closely spaced serine and threonine residues prevented the assignment of additional phosphorylation sites to specific residues, we performed mass spectrometry using a panel of AGO2 alanine mutants sparing subsets of these putative phosphorylation sites. This allowed definitive identification of phosphorylation at S828 and S831 (Figure 21c,d). Confirming the correct identification of the relevant phosphorylation sites, mutating all five serine/threonine residues in this region to alanine (5xA) completely abolished the p-AGO2 band observed by Phos-tag (Figure 22). Interestingly, a single S828A mutation also fully abolished the AGO2 mobility shift, suggesting that phosphorylation of this residue may be necessary to trigger phosphorylation of additional amino acids within this region in a hierarchical manner.

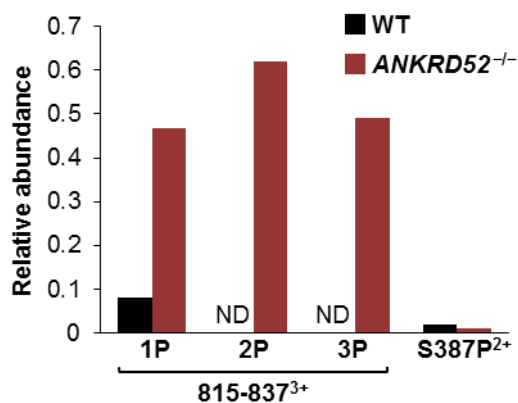


Figure 19: Mass spectrometry reveals enhanced phosphorylation of AGO2 at S824-S834. Quantification of the indicated endogenous AGO2 phosphopeptides relative to unphosphorylated peptide as determined by mass spectrometry. 1P, 2P, or 3P respectively denotes singly, doubly, or triply phosphorylated peptides spanning residues 815-837 of AGO2. Superscript indicates peptide charge state. ND, not detected.



Figure 20: Evolutionary conservation of AGO2 S824-S834. Putative phosphorylation sites shown in red.

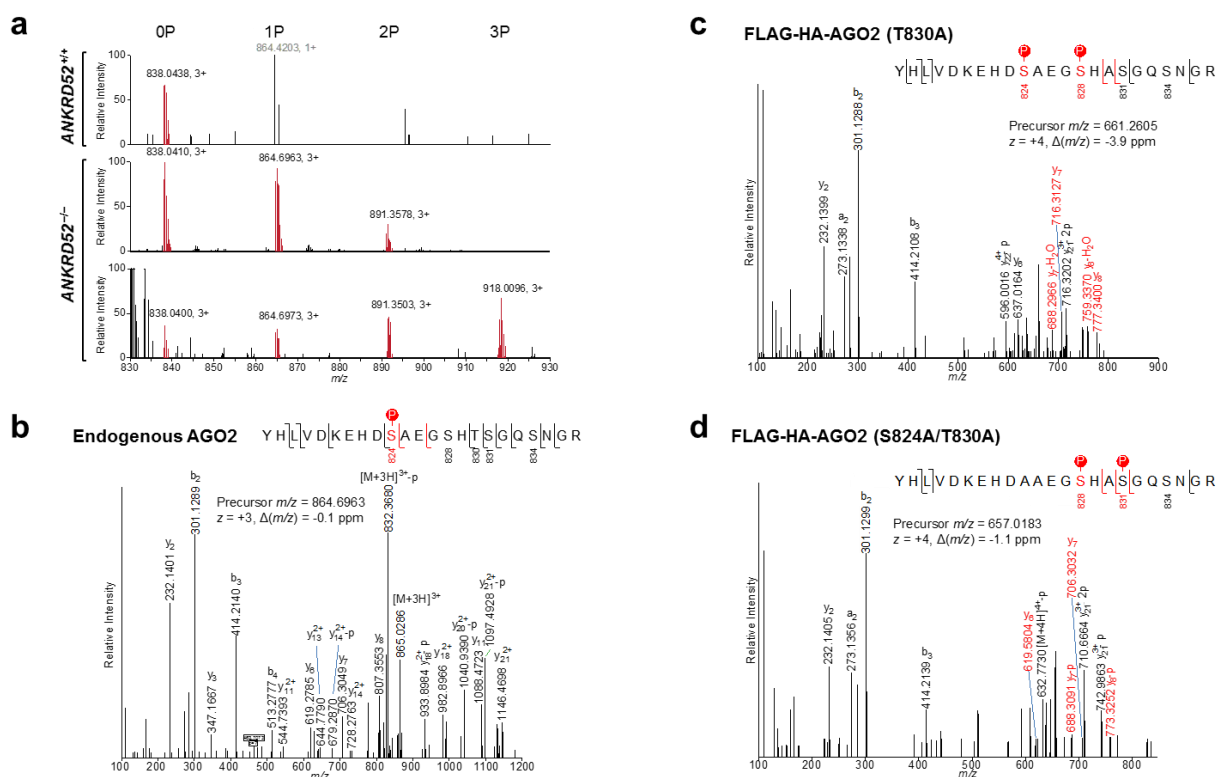


Figure 21: Identification of multiple definitively phosphorylated residues in the S824-S834 region of AGO2 by mass spectrometry. a, Full scan mass spectra zoomed to the region for the AGO2 815-837 peptide. The unphosphorylated and multiply phosphorylated precursor ions are shown in red. Peak labels indicate the mass-to-charge ratios and the charge state. The singly charged ion with grey label (top panel) does not correspond to peptide 815-837. Data at two close elution time points are shown for ANKRD52^{-/-} to illustrate the unphosphorylated (0P), singly (1P), doubly (2P) and triply (3P) phosphorylated peptides. **b**, MS/MS spectra demonstrating phosphorylation of endogenous AGO2 at S824 in ANKRD52^{-/-} cells. Red bars denote site-determining ions. **c**, **d**, MS/MS spectra demonstrating phosphorylation of FH-AGO2 (T830A) at S824 and S828 (**c**) or phosphorylation of FH-AGO2 (S824A/T830A) at S828 and S831(**d**) in ANKRD52^{-/-} cells.

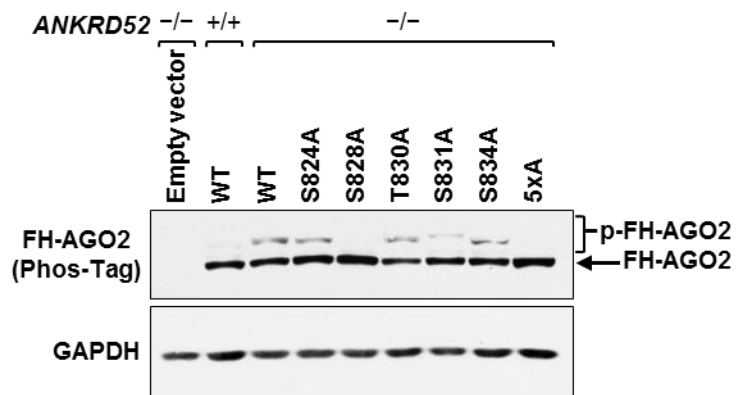


Figure 22: AGO2 phosphorylation is abolished by either an S828A mutation or a 5xA mutation. Phos-tag analysis of FH-AGO2 mutants stably expressed in *ANKRD52*^{-/-} cells.

We postulated that hyperphosphorylation of S824-S834 inhibits AGO2 activity, thus accounting for the defect in miRNA-mediated silencing in ANKRD52/PPP6C-deficient cells. The human AGO2 crystal structure revealed that the S824-S834 region is within an unresolved loop of the PIWI domain that is located in the vicinity of the miRNA:mRNA target interface (89, 90). We therefore hypothesized that phosphorylation in this region may reduce the association of AGO2 with miRNAs and/or targets. Immunopurification of endogenous AGO2 from *ANKRD52*^{+/+} or *ANKRD52*^{-/-} cells demonstrated equivalent miRNA association (Figure 23a). In contrast, AGO2:mRNA target association was dramatically reduced in *ANKRD52*^{-/-} cells, as determined by assessing AGO2 binding to the miR-19 *EGFP* reporter mRNA and two established endogenous mRNA targets of different miRNAs (Figure 23b) (91, 92).

To further demonstrate that phosphorylation of AGO2 at S824-S834 inhibits target association, we used an established protocol (93) to capture AGO2:miRNA complexes with an RNA oligonucleotide that mimics a target of miR-21, an abundant miRNA in HCT116 cells (94) (Figure 24). Whereas unphosphorylated AGO2 was efficiently recovered using this approach, the ability of the phosphorylated form to bind to the synthetic target was dramatically decreased (Figure 25). Importantly, both phosphorylated and unphosphorylated forms of AGO2 were efficiently recovered by immunoprecipitation using an anti-AGO2 antibody, demonstrating that the relevant phosphoresidues were stable under these purification conditions.

To identify the specific phosphoresidues that impair AGO2 target association, we expressed a series of phosphomimetic mutants and assessed their target binding activity. As expected, none of the mutations measurably decreased miRNA association

(Figure 26). In contrast, we found that target association was significantly impaired by several of these substitutions, including glutamate mutations of all five serine and threonine residues in the S824-S834 region (5xE) and, more importantly, individual mutations or combinations of mutations that mimic definitive phosphorylation sites documented by mass spectrometry (S831E, S828E/S831E, and S824E/S828E/S831E) (Figure 27). Interestingly, mutation of all serines and threonines in this region to alanine (5xA) enhanced target association, suggesting that phosphorylation of wild-type AGO2 detectably inhibits target association at baseline.

To test whether phosphorylation of S824-S834 impacts other aspects of AGO2 function in addition to target binding, we used the λ N peptide-boxB system (95) to tether wild-type or mutant AGO2 to a luciferase reporter transcript. Both wild-type and 5xE λ N-AGO2 displayed equivalent silencing activity in this assay (Figure 28), demonstrating that these mutations result in an isolated defect in target binding but do not otherwise affect AGO2 activity. Taken together, these findings establish that phosphorylation of S824-S834 represents a potent and specific mechanism through which the ability of AGO2 to bind target mRNAs is regulated.

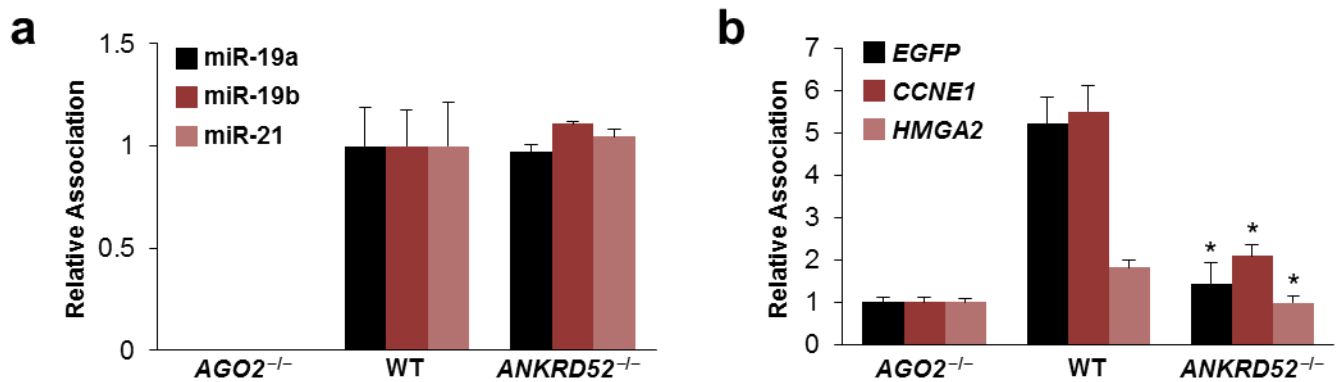


Figure 23: AGO2 phosphorylation impairs mRNA target association but spares miRNA association. **a**, Measurement of AGO2-associated miRNA by qRT-PCR. miRNA recovery was normalized to the amount of AGO2 recovered and then normalized to wild-type value. Average values from two biological replicates each assayed in triplicate shown. Error bars indicate SD for this and all subsequent qRT-PCR data. **b**, AGO2-target association assessed as described in (a). * $p < 0.05$, Student's t test comparing *ANKRD52*^{-/-} to WT.

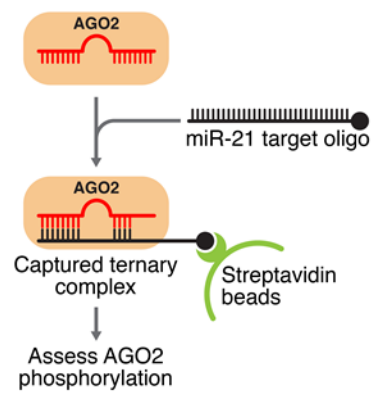


Figure 24: AGO2 can be captured from cell lysates using a bait target oligonucleotide. Schematic of AGO2:miRNA target capture experiment.

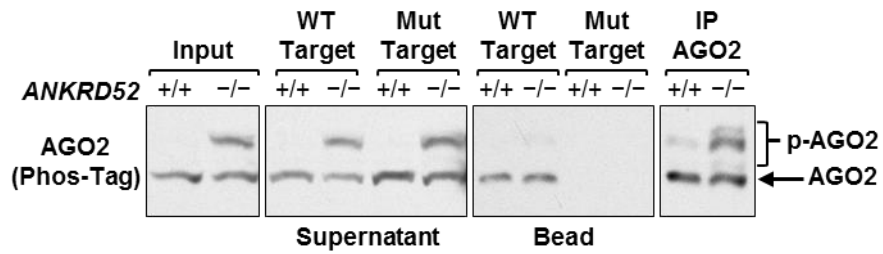


Figure 25: An mRNA target mimic selectively captures non-phosphorylated AGO2. Phos-tag western blot demonstrating impaired association of hyperphosphorylated AGO2 with target oligonucleotide.

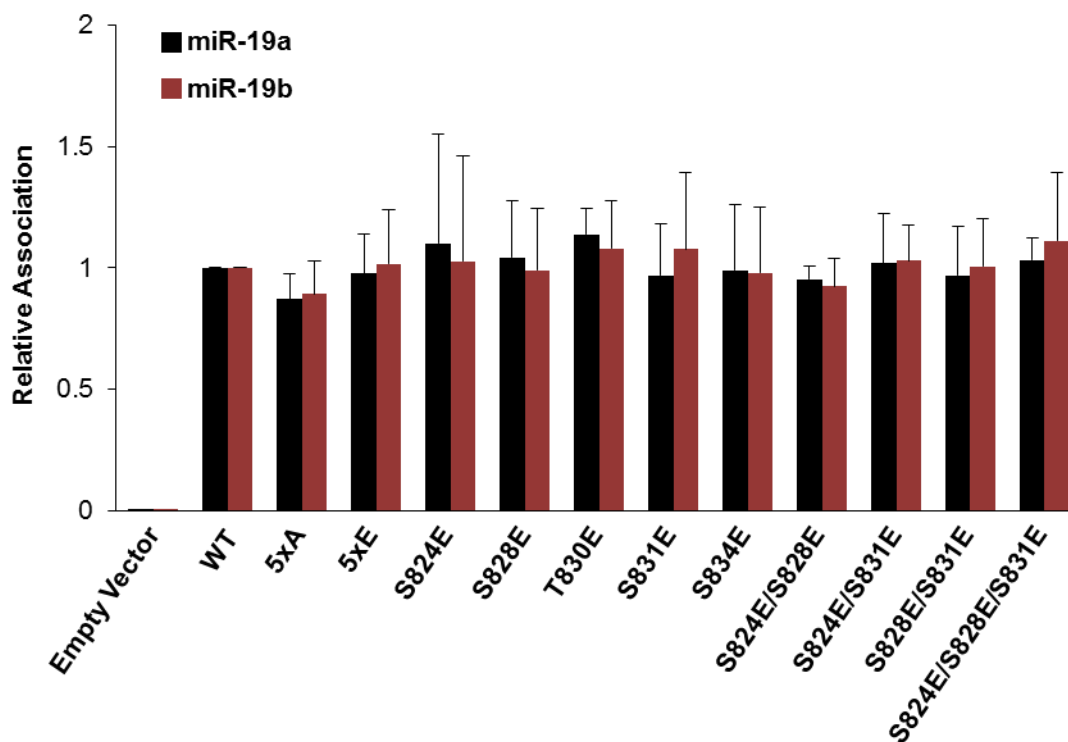


Figure 26: Phosphomimetic mutants of FH-AGO2 do not exhibit reduced miRNA association. miRNA association of wild-type or mutant FH-AGO2 assessed as described in Figure 23 ($N = 4$ biological replicates, each assayed in triplicate).

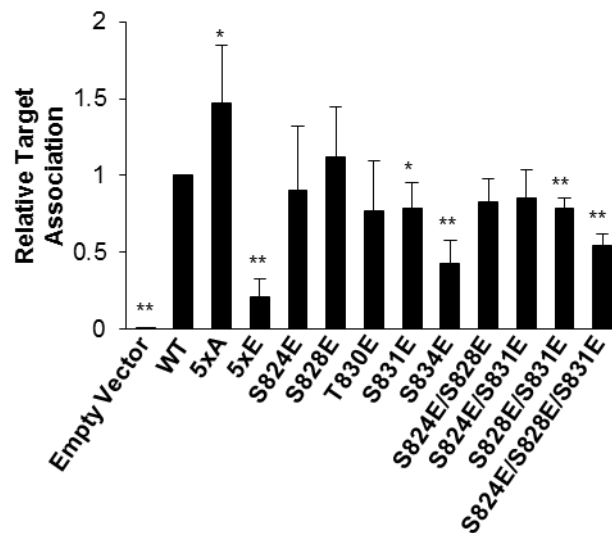


Figure 27: Phosphomimetic mutants of FH-AGO2 exhibit reduced mRNA association. mRNA association (EGFP miR-19 reporter transcript) of wild-type or mutant FH-AGO2 assessed as described in Figure 23 ($N = 4$ biological replicates, each assayed in triplicate).

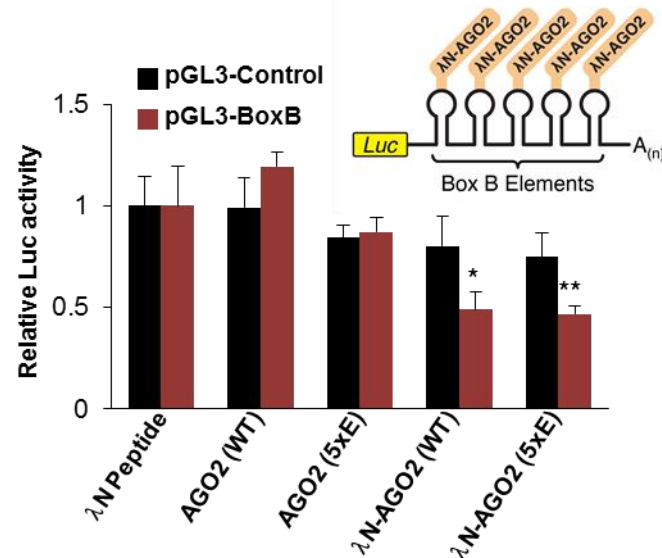


Figure 28: A phosphomimetic mutant of AGO2 is competent to silence mRNA targets when directly tethered. Schematic representation of AGO2 tethering experiments and results of luciferase assays demonstrating repression of luciferase-BoxB (pGL3-BoxB) by λ N-AGO2 (WT) and λ N-AGO2 (5xE), but not by untethered AGO2 or λ N alone. A luciferase transcript lacking BoxB sites (pGL3-Control) served as a negative control. * $p < 0.05$; ** $p < 0.01$, Student's t test ($N = 3$ biological replicates).

Having identified the phosphatase arm of this new AGO2 phosphorylation cycle, we next sought to identify the kinase that initiates this inhibitory mechanism. Reasoning that loss of function of the kinase would rescue miRNA-mediated silencing in the ANKRD52-deficient state, we performed a secondary genome-wide CRISPR-Cas9 screen in *ANKRD52*^{-/-} HCT116^{EGFP-miR19} cells and collected the dimmest 0.5% of cells (Figure 29). RIGER analysis revealed four serine/threonine kinases among the top 100 hits: *LATS2*, *CSNK1A1*, *mTOR*, and *SRPK1* (Figure 30, Table 4 of Appendix). Knockout of *LATS2* or *SRPK1* in the *ANKRD52*^{-/-} background resulted in minimal recovery of EGFP repression (Figures 31a, b). mTOR knockout or inhibition with rapamycin moderately rescued EGFP repression but did not influence AGO2 phosphorylation (Figures 31c, d). In stark contrast, knockout of *CSNK1A1* in *ANKRD52*^{-/-} cells (Figure 32) fully rescued repression of the *EGFP* reporter without increasing miR-19 levels (Figures 33a, 34), greatly reduced AGO2 phosphorylation (Figure 33b), and restored AGO2 target association (Figure 33c).

Co-immunoprecipitation demonstrated an RNA-independent interaction between CSNK1A1 and AGO2 (Figure 35), supporting a direct role for CSNK1A1 in AGO2 phosphorylation. Moreover, the casein kinase I (CKI) family, of which CSNK1A1 is a member, prefers previously phosphorylated substrates conforming to the consensus (pS/pT/D/E)-X₁₋₂-S/T, with the latter S/T representing the phospho-acceptor site(96, 97). Notably, the five serine/threonine residues within AGO2 S824-S834 all conform to this consensus motif, with S824 and S828 preceded by acidic residues and T830, S831, and S834 having the potential to be primed by hierarchical phosphorylation initiating at S828. To directly determine whether full-length AGO2 is a direct substrate of

CSNK1A1, wild-type AGO2 or the 5xA mutant was purified from human cells, treated with lambda phosphatase to remove potential priming phosphorylation events, and incubated with recombinant CSNK1A1 *in vitro*. Under these conditions, phosphorylation of wild-type but not 5xA AGO2 by CSNK1A1 was clearly detectable (Figure 36a). To further explore the potential for hierarchical phosphorylation in this region, CSNK1A1 kinase assays were performed with a series of peptides containing phosphoserines at positions corresponding to S824, S828, and S831 of AGO2 (Figure 36b).

Unphosphorylated peptide was a poor substrate for CSNK1A1 under these conditions, suggesting that initial phosphorylation of this region is facilitated by contextual features present in full-length AGO2. Likewise, pS824 only weakly stimulated further phosphorylation of this peptide. In contrast, prior phosphorylation of S828 robustly promoted phosphorylation of S831 (but not T830), while pS831 efficiently primed phosphorylation of S834. Taken together with our earlier data demonstrating a critical role for S828 in phosphorylation of AGO2 in whole cells (Figure 22), these findings support a model whereby initial phosphorylation of S828, and potentially S824, by CSNK1A1 is an inefficient event, perhaps stimulated by conformational changes in AGO2 or yet-to-be defined additional priming kinases or co-factors. Once phosphorylated, however, pS828 stimulates efficient hierarchical phosphorylation of S831 followed potentially by S834 by CSNK1A1, rendering AGO2 incompetent for target binding until returned to an active state by the phosphatase activity of the ANKRD52-PPP6C complex (Figure 37).

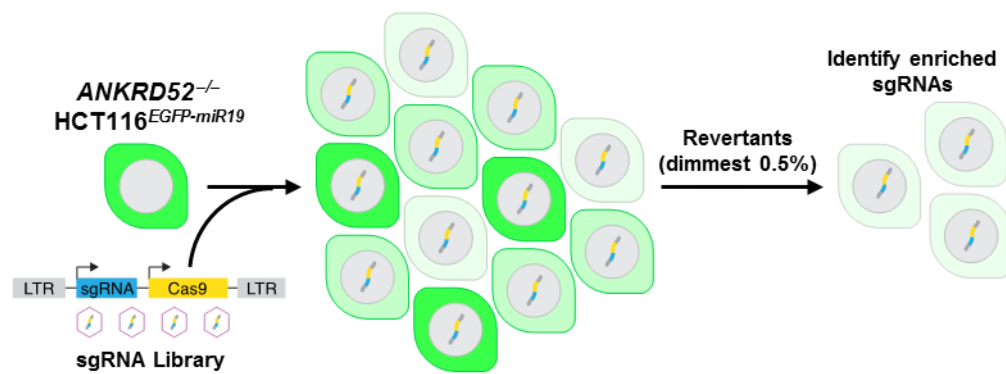


Figure 29: Design of a CRISPR-Cas9 screen to identify suppressors of the *ANKRD52*^{-/-} phenotype.

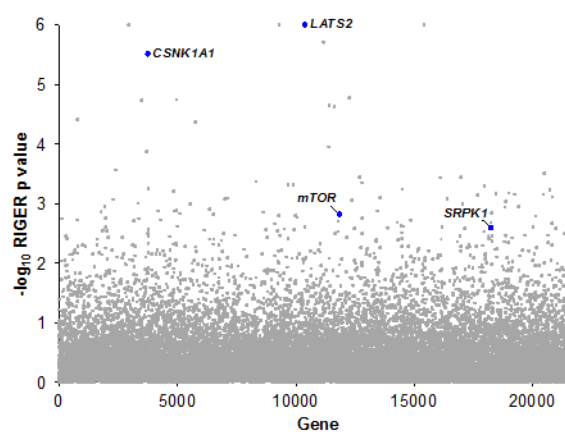


Figure 30: Four serine/threonine kinases emerge as hits from a genome-wide CRISPR-Cas9 suppressor screen. RIGER analysis of screening results with serine/threonine kinases highlighted.

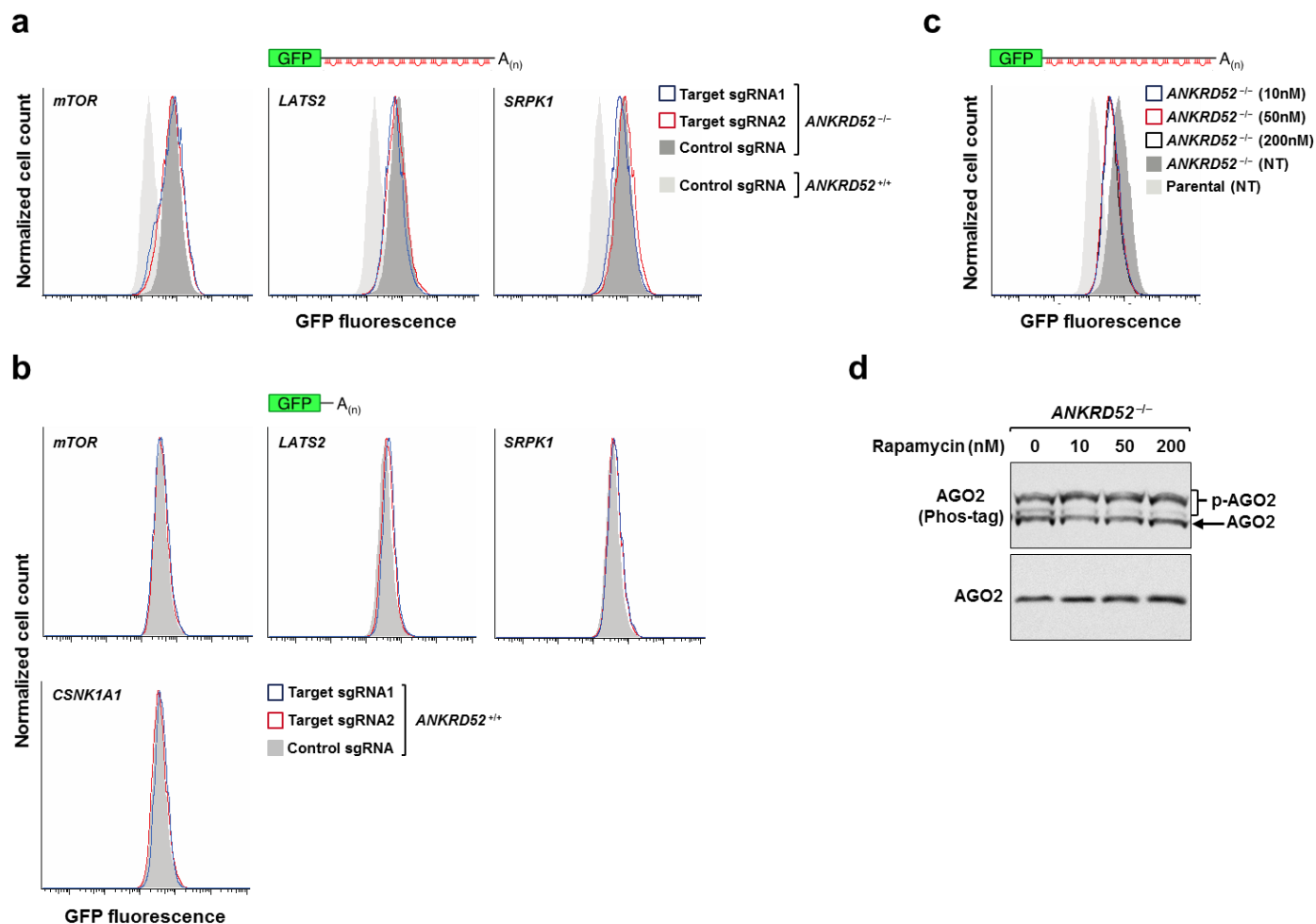


Figure 31: Analysis of three serine/threonine kinases identified in the CRISPR-Cas9 suppressor screen. a, b, Flow cytometry demonstrating EGFP expression in HCT116^{EGFP-miR19} (a) or HCT116^{EGFP} cells (b) after transduction with lentiCRISPR vectors targeting the indicated genes. (c), Flow cytometry demonstrating EGFP expression in HCT116^{EGFP-miR19} cells treated with the indicated dose of rapamycin. NT, not treated. (d), Phos-tag western blot analysis of AGO2 in ANKRD52^{-/-} cells after treatment with rapamycin.

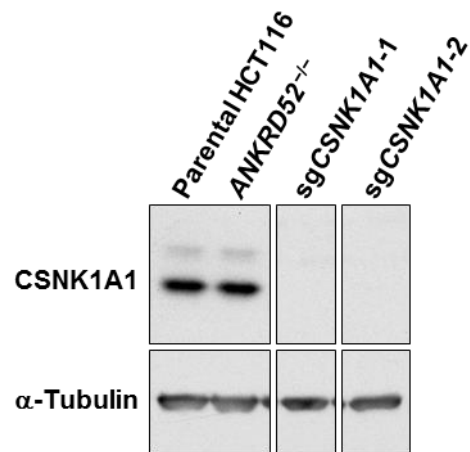


Figure 32: Characterization of ANKRD52^{-/-}; CSNK1A1^{-/-} cells. Western blot analysis confirms loss of CSNK1A1 expression in HCT116 ANKRD52^{-/-}; CSNK1A1^{-/-} clonal knockout cells. All lanes came from the same blot but irrelevant lanes were removed.

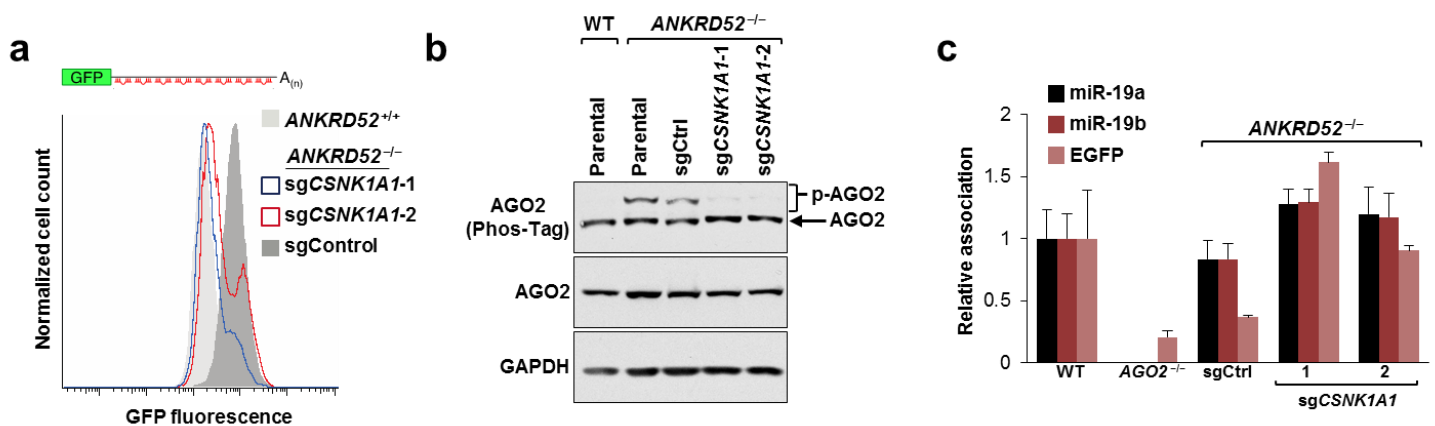


Figure 33: A CRISPR-Cas9 suppressor screen reveals CSNK1A1 as the inhibitory AGO2 kinase. **a**, Flow cytometry demonstrating rescued repression of EGFP in *ANKRD52*^{-/-} HCT116^{EGFP-miR19} cells transduced with lentiCRISPR vectors targeting *CSNK1A1*. **b**, Phos-tag electrophoresis reveals a strong reduction of phosphorylated AGO2 in *ANKRD52*^{-/-}; *CSNK1A1*^{-/-} cells. **c**, Relative association of miR-19a, miR-19b and EGFP target mRNA with AGO2 was assessed as described in Fig. 3a (*N* = 3 biological replicates).

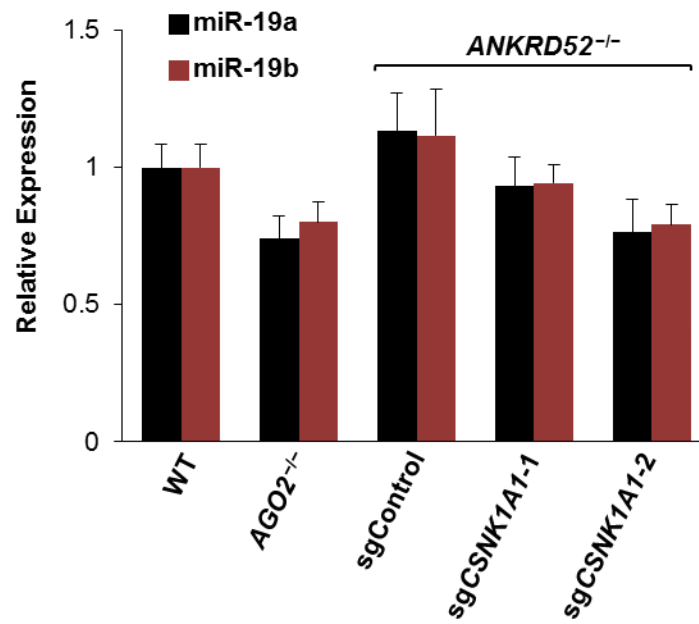


Figure 34: Characterization of miR-19 expression in *ANKRD52*^{-/-}; *CSNK1A1*^{-/-} cells. miR-19 expression normalized to U6 expression, assessed by qRT-PCR, in cells of the indicated genotypes ($N = 4$ biological replicates, each assayed in triplicate).

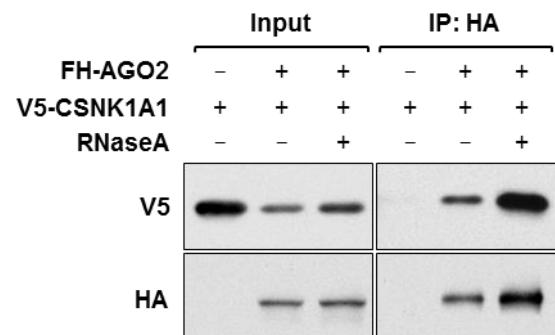


Figure 35: AGO2 and CSNK1A1 interact in an RNA-independent manner. Co-immunoprecipitation of V5-CSNK1A1 with FH-AGO2, with or without RNase A treatment.

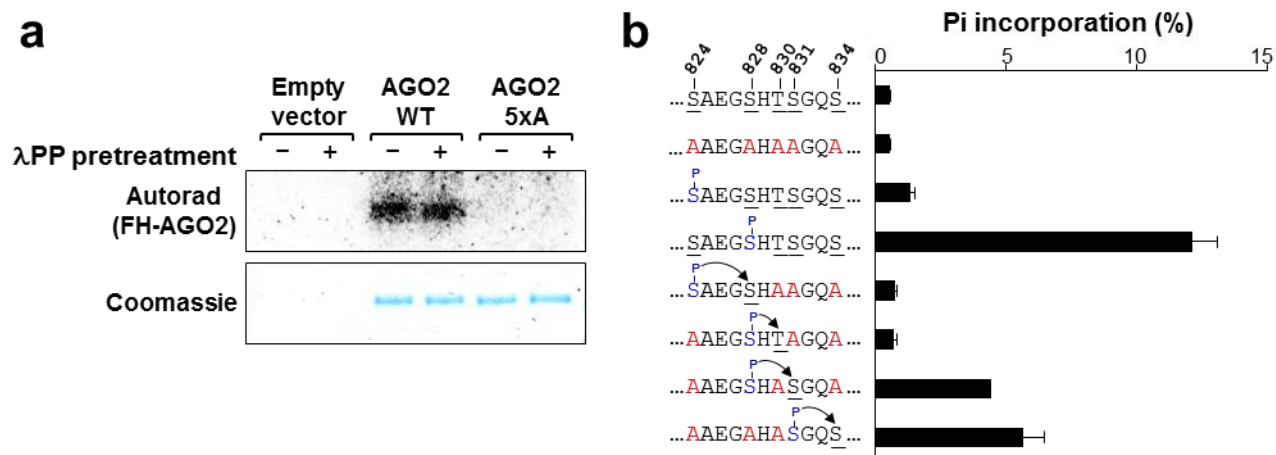


Figure 36: AGO2 is a direct substrate of CSNK1A1. **a**, *In vitro* CSNK1A1 kinase assays showing phosphorylation of full-length WT FH-AGO2 but not 5xA FH-AGO2 with or without pre-treatment with λ PP. **b**, *In vitro* CSNK1A1 kinase assays demonstrating phosphorylation of peptides containing AGO2 S831 and S834 when primed by pS828 and pS831, respectively.

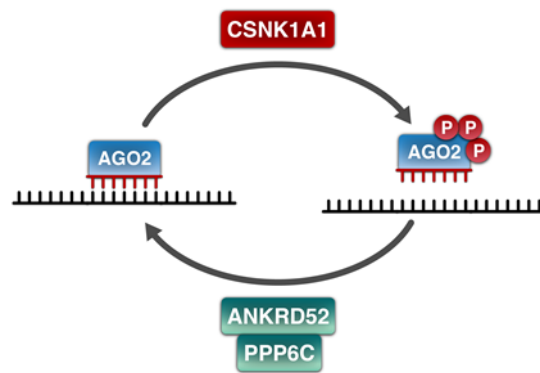


Figure 37: An AGO2 phosphorylation cycle regulates target mRNA engagement.

Discussion

CRISPR-Cas9 screening in the HCT116^{EGFP-miR19} cells revealed both global regulators of the pathway as well as specific regulators of the miR-17-92 cluster. A genetic suppressor screen using similar methods yielded additional regulators of miRNA function. Taken together, the results of these genetic screens demonstrate the feasibility and powerful sensitivity of coupling fluorescent reporters of miRNA activity to established CRISPR-Cas9 screening libraries. We anticipate that these methods may be extended to study the regulation of many other regulatory networks governing miRNA function. More broadly, these methods may be adapted to dissect the regulatory architecture of other molecular pathways by modifying the design of the fluorescent reporter.

Global dysregulation of the miRNA pathway can significantly disturb mammalian development and compensatory responses to stress (37, 98, 99). Elucidating the regulatory machinery that has evolved to tune the activity of the pathway remains a major priority. Although some regulatory mechanisms are invoked in response to acute stimuli, others are necessary for optimal function of the pathway under baseline conditions (63, 65). Here we have presented compelling evidence for an AGO2 phosphorylation cycle that can regulate the pathway at the level of target association. Loss of the phosphatase arm of the cycle strongly impairs global miRNA function under normal growth conditions and genetic ablation of the AGO2 kinase, CSNK1A1, rescues silencing of a miR-19 reporter.

The existence of this Argonaute phosphorylation cycle now begs further interrogation into the biological contexts where cells engage the pathway to modify

silencing activity. Tracking AGO2 phosphorylation across organismal development and examining the tissue-specific accumulation of p-AGO2 would provide a broad characterization of the potential contexts in which the levels of unphosphorylated AGO2 and p-AGO2 are altered. Similarly, surveying AGO2 phosphorylation under conditions known to acutely impair the pathway may provide deeper insight into the contexts in which the cycle functions to maintain homeostasis (100). Perhaps a more significant way to reveal the functions of the Argonaute phosphorylation cycle will be to engineer mice carrying phosphomimetic or phosphomutant versions of AGO2. Undoubtedly, further characterization of this novel cycle will clarify the importance of Argonaute phosphorylation in organismal homeostasis.

CHAPTER THREE

Discussion

Review of findings

Elucidating biologically significant regulatory mechanisms of the miRNA pathway remains a major priority for the field. We have characterized a previously unappreciated regulatory phosphorylation cycle for Argonaute by elucidating necessary components of both the kinase and phosphatase arms of the cycle. These studies have also unveiled a regulatory architecture for the transcriptional regulation of the miR-17-92 cluster, with particular focus on the biogenesis of miR-19.

Novel transcriptional regulators of the miR-17-92 cluster

The miR-17-92 cluster remains perhaps one of the most intensely studied miRNA clusters with respect to development and oncogenesis in mammals. Hemizygous loss of the miR-17-92 cluster leads to developmental abnormalities in humans (38). Engineered mutations in mice recapitulate many of these effects, including microcephaly and digital abnormalities. Complete loss of the cluster is incompatible with life for mice (39). Mice with homozygous loss of the cluster exhibit hypoplastic lungs, abnormal cardiac structures, and impaired B cell maturation. Notably, the miR-17-92 cluster is not alone among miRNA knockout mice demonstrating overt development abnormalities. Deletion of members of the miR-196 family drives altered vertebral morphology in mice (101). Mice deficient in miR-140 exhibit short stature, a finding consistent with the selective expression of miR-140 in the cartilage (102).

The oncogenic role for the miR-17-92 cluster was established using animal models after early reports observed significant amplification of this non-coding RNA cluster in patient-derived tumor samples (103). Lin He and colleagues demonstrated an *in vivo* role for the cluster in mediating Myc-driven lymphomagenesis in mice (45). Further studies carefully dissected the contributions of individual miRNAs within the cluster in promoting oncogenesis. The loss of miR-19 alone was sufficient to significantly reduce the progression of Myc-driven lymphomagenesis and Myc-driven adenocarcinoma of the prostate in mice (47). In sum, miR-19 alone is a significant contributor to the oncogenic phenotype associated with expression of the miR-17-92 cluster.

Given the significant biological role for miR-19 in oncogenesis, identifying regulators of this miRNA alone could have significant implications for therapies targeting Myc-driven oncogenic events. Our initial CRISPR-Cas9 loss-of-function screen to identify novel regulators of the miRNA pathway was sensitive to global regulators of the pathway, as well as specific regulators of miR-19. Further studies identified a transcriptional network governing the expression of the pri-miR-17-92 transcript. *MYC* is known to be a central driver of transcription of pri-miR-17-92 (49). Genetic ablation of *CTNNB1* or *BRD4* results in nearly a 50% reduction in *MYC* transcript levels and a similar reduction in pri-miR-17-92 expression, consistent with reduced transcription of the cluster. Curiously, mature miR-19a and miR-19b were both reduced approximately 80% in *BRD4* knockout cells, but loss of *CTNNB1* only reduced expression of these miRNAs by 50%. This discrepancy suggests that *BRD4* may promote the biogenesis or stability of these miRNAs through an alternative mechanism in addition to promoting

MYC-driven expression of the host transcript. Future studies should involve surveying the global miRNA landscape to determine if there is a widespread reduction in mature miRNA expression in *BRD4*^{-/-} cells. If a global deficit is present, assessing the various stages of miRNA biogenesis and evaluating the half-lives of mature miRNAs would be appropriate angles of inquiry to begin dissecting the relevant deficiencies in the pathway.

The initial CRISPR-Cas9 screen also demonstrated a role for *POU2F1*, also known as *OCT1*, in promoting the biogenesis of mature miR-19. Loss of *POU2F1* did not reduce *MYC* expression, suggesting that this transcription factor promotes biogenesis perhaps by binding directly to the promoter for pri-miR-17-92. An earlier report studying the transcription of the miR-17-92 cluster identified a putative binding site for an OCT protein family member in the promoter for the miRNA (104). Mutation of this site reduced expression of a luciferase reporter approximately 50%. Interpreting this study in the context of our loss-of-function studies of *POU2F1* strongly implicates pri-miR-17-92 as a direct transcriptional target of *POU2F1*. Further studies demonstrating direct binding of *POU2F1* to the pri-miR-17-92 promoter would further support this hypothesis.

Our development of a CRISPR-Cas9 screening platform for regulators of the miRNA pathway provides a powerful tool for dissecting the transcriptional networks governing the expression of particular miRNAs. This study identified at least three genes that are involved in promoting the transcription of the pri-miR-17-92 cluster. The transcriptional networks governing the expression of other miRNAs could be studied by simply replacing the miRNA binding sites in the EGFP reporter with binding sites to

other miRNAs that are expressed at consequential levels. Varying the cell type in which the CRISPR-Cas9 loss-of-function screen is performed would allow for the identification of transcriptional regulators of a miRNA within a specific cell type. These potential variations on the initial screen highlight the flexibility of this screening approach, and the results obtained in the initial screen confirm its functionality for identifying regulators of specific miRNAs.

A novel phosphorylation cycle for AGO2

A second class of hits emerged from the screen, regulators of global miRNA function. Many known components of the canonical miRNA biogenesis pathway emerged (2). These include, but are not limited to, *DROSHA*, *DGCR8*, *DICER1*, and *XPO5*. The presence of these genes as highly enriched hits from the screen confirmed the sensitivity of the screen for major molecular components of global miRNA function. Two components of a phosphatase complex, *ANKRD52* and *PPP6C*, were revealed to be highly significant hits from the screen as well (86). This observation led us to characterize the consequences for miRNA silencing when this complex is knocked out in human cells.

To study the extent to which the protein phosphatase 6 (PP6) complex regulates miRNA function, clonal knockout cell lines were derived for *ANKRD52*. Attempts to generate clonal knockout cell lines for *PPP6C* were hampered by significant toxicity elicited upon loss of *PPP6C*. RNA sequencing analysis confirmed significant upregulation of multiple mRNAs in *ANKRD52*^{-/-} that are also elevated in cells deficient for *AGO2*. These results strongly support a role for *ANKRD52* in promoting global

function of the pathway. Mass spectrometry analysis allowed us to identify a region within AGO2 that becomes highly phosphorylated in the absence of *ANKRD52* or *PPP6C*. Further studies demonstrated that AGO2 cannot associate efficiently with mRNA targets when the protein is phosphorylated in this region, despite miRNA association remaining relatively unchanged. Collectively, these observations suggest that the AGO2:miRNA complex can undergo temporary inactivation by phosphorylation at the S824-S834 region. The existence of an on/off switch that preserves miRNA association could allow the cell to rapidly, but reversibly, downregulate the miRNA pathway. Such a mechanism could be relevant for signaling cascades, development, and acute stress responses.

Identifying stimuli of AGO2 phosphorylation could reveal contexts in which inactivation of the miRNA pathway occurs and promotes a homeostatic response to some initiating event. Elucidating the kinase or kinases responsible for AGO2 phosphorylation could provide information about potential stimuli for phosphorylation. A genome-wide suppressor screen in EGFP miR-19 reporter cells deficient for *ANKRD52* identified *CSNK1A1* as the relevant AGO2 kinase. Although alternative splicing and miRNA-mediated gene silencing are both known to regulate *CSNK1A1* (105), the activity of the enzyme is not known to be strongly and acutely regulated by cell signaling events. In this case, identifying the AGO2 kinase as *CSNK1A1* did not immediately provide leads as to potential stimuli for AGO2 phosphorylation.

The CRISPR-Cas9 genome-wide suppressor screen also identified *LATS2* and *mTOR* as potential AGO2 kinases. Loss of either kinase partially rescues silencing of the EGFP miR-19 reporter in *ANKRD52*^{-/-} cells. However, knockout of either *LATS2* or

mTOR failed to rescue the hyperphosphorylation of AGO2 observed by Phos-tag western blotting. These kinases may regulate the miRNA pathway through an alternative mechanism. These observations leave open the possibility that other kinases could still directly phosphorylation AGO2 at the S824-S834 region. Factors such as genetic redundancy, knockout toxicity, and ineffective sgRNAs may have led to *CSNK1A1* being the only AGO2 kinase identified from the screen. Further investigation aimed at identifying additional kinases for AGO2 would be feasible given the development of novel genome-wide gene activation screening systems (106). One could perform a genome-wide CRISPR-Cas9 activation to determine if overexpression of a single kinase could drive AGO2 phosphorylation.

Deriving phospho-specific antibodies against p-AGO2 would provide useful tools for analyzing the relative levels of p-AGO2 across various tissues, developmental points, or disease states. Our work has identified at least three definitively phosphorylated residues within the S824-S834 loop. These include S824, S828, and S831. *In vitro* kinase assays also suggest that S834 may be directly phosphorylated by *CSNK1A1* if AGO2 is phosphorylated at S831. Deriving phospho-specific antibodies against each of these four sites would yield a useful toolkit for finely dissecting relative levels of phosphorylation and the kinetics of phosphorylation within the S824-S834 loop. Successful phospho-specific antibody production may also allow one to immunoprecipitate p-AGO2 and search for novel protein and/or RNA interactions. Although we anticipate p-AGO2 is inactive with respect to its miRNA-mediated silencing function, there may be additional functions of p-AGO2 that are yet to be appreciated.

The deep evolutionary conservation of the pS824-pS834 loop (107) suggests that Argonaute proteins in other organisms, such as *D. melanogaster* and *C. elegans*, may regulate Argonaute activity through phosphorylation of this region. Identifying orthologues of *ANKRD52*, *PPP6C*, and *CSNK1A1* in other organisms could then be coupled to loss-of-function studies and analysis of the phosphorylation state of Argonaute. Semi-quantitative mass spectrometry and/or Phos-tag western blots could be employed to assess Argonaute's phosphorylation status. Analysis of miRNA function under such genetic manipulations would also help determine if similar molecular components are used to regulate the activity of Argonaute in other organisms. Studying Argonaute phosphorylation in other model organisms may also facilitate *in vivo* experiments that reveal the global consequences for an organism with deficiencies in the Argonaute phosphorylation cycle.

Characterizing the *in vivo* significance of AGO2 phosphorylation could be accomplished through murine models. Phosphomutant and phosphomimetic versions of *AGO2* could be knocked into the mouse genome (108), and the consequences for development and baseline homeostasis could be assessed in animals. A phosphomimetic mutant of *AGO2* would be expected to demonstrate significantly impaired function with respect to promoting miRNA activity. The expression of *AGO2* is essential for mouse development (98), and the loss of various miRNAs impairs proper development (39, 101, 102). A phosphomimetic mutant of *AGO2* may demonstrate altered development if the activity of the miRNA pathway is globally dysregulated.

In vivo studies targeting the elucidated components of the *AGO2* phosphorylation cycle may also stimulate an appreciation for the biological significance of the cycle. For

example, *PPP6C* is commonly mutated in melanoma and basal cell carcinoma (109, 110). Genetic ablation of *PPP6C* accelerates ultraviolet-B-induced skin carcinogenesis and accelerates chemically-induced skin carcinogenesis as well (111, 112). CRISPR-Cas9 targeting of *ANKRD52* in mouse non-small cell lung cancer cells accelerates primary tumor growth in mice (113). Loss of heterozygosity for *CSNK1A1* in mice deficient for p53 in the gut results in invasive carcinoma (114). Each of these findings linking loss-of-function of the one of the critical regulators of AGO2 phosphorylation to accelerated oncogenesis provides an opportunity to investigate the potential contributions of dysregulated miRNA function to each phenotype.

Numerous situations could exist in which AGO2 phosphorylation is altered in either a compensatory or pathological manner. However, understanding the fundamental necessity for the AGO2 phosphorylation cycle remains a paramount priority. Loss of either *ANKRD52* or *PPP6C* clearly traps Argonaute in a hyperphosphorylated and inhibited state in which mRNA target association is strongly reduced. However, loss of *CSNK1A1*, a kinase essential for the phosphoinhibition of AGO2, has only been demonstrated to fully rescue repression of the EGFP miR-19 reporter in *ANKRD52*-deficient cells. More comprehensive transcriptome-wide analysis will be necessary to see if loss of this kinase globally rescues miRNA-mediated silencing. Perhaps deletion of *CSNK1A1* alone or expressing 5xA phosphomutant AGO2 in AGO2-deficient cells would result in perturbed miRNA function. These experiments could provide direct support for the necessity of AGO2 phosphorylation in maintaining efficient function of the pathway.

Adapting fluorescent reporters and CRISPR-Cas9 screening to dissect other pathways

A final lasting contribution of this work to the broader scientific community includes the development of a flexible screening platform for dissecting the machinery of molecular pathways using fluorescent reporters and established CRISPR-Cas9 genome-scale libraries (5, 6). Several parameters of the initial CRISPR-Cas9 screen were chosen after rounds of iterative experimentation and data analysis in collaboration with Dr. Yang Xie's lab at UT Southwestern. Experimental measurements of knockout efficiency and reporter responsiveness were generated, and the analysis of these data guided our selection of precise gates for FACS analysis. Library preparation and sequencing parameters were optimized with significant assistance from Dr. Vanessa Schmid at the Eugene McDermott Center for Human Growth and Development. The published technical methods for conducting a genome-scale CRISPR-Cas9 screen using the approaches derived in this work may be adapted by other groups. Fluorescent reporters could be designed to measure such processes as gene transcription, post-transcriptional regulation, and the post-translational regulation of proteins fused to EGFP. These reporters could then be coupled to the methods established in this study for detecting regulators of a biological process.

Summary

Despite over a decade of intensive study, mechanisms that regulate miRNA-mediated silencing are incompletely understood. By applying iterative rounds of genome-wide CRISPR-Cas9 screening to this problem, we have uncovered a new AGO2 phosphorylation cycle that potently regulates target mRNA engagement. The

deep conservation of the relevant phosphorylation sites in metazoan Argonaute proteins suggests that this mechanism is broadly utilized to regulate the pathway in diverse species. Moreover, these findings demonstrate that miRNA abundance or loading into Argonaute proteins does not necessarily equate with miRNA silencing activity, highlighting target association as a major level of control of the pathway. We anticipate that the highly flexible fluorescent marker-based CRISPR-Cas9 screening strategy described here will facilitate the functional dissection of other important biological pathways directly in human cells.

CHAPTER FOUR

Methods

Construction of miR-19 reporter

EGFP was PCR amplified from EGFP-hAGO2 (Addgene #21981) and cloned into pMSCV-Puro (Clontech) using the BglII and XhoI restriction sites. The puromycin resistance cassette was then removed by EcoRI and ClaI digestion and replaced with an insert containing eight imperfect miR-19 binding sites [modeled from (78)], synthesized as a gBlock (IDT) (sequence in Appendix, Table 5). For EGFP only reporter, the puromycin resistance cassette was removed by EcoRI and ClaI digestion followed by re-ligation after filling-in overhangs.

Generation of HCT116 reporter cell lines

MSCV-EGFP and MSCV-EGFP-miR-19 retrovirus was generated by first seeding 6×10^5 cells per well in a 6-well dish. The following day, cells were transfected using 1 μg of plasmid (MSCV-EGFP or MSCV-EGFP-miR-19), 3 μL of FuGENE HD (Promega), and 200 μL Opti-MEM (Thermo Fisher) per well according to manufacturer's instructions. Media was changed the next day. Two days after transfection, media was collected and passed through a 0.45 μm SFCA sterile filter. Recipient HCT116 cells were transduced overnight at an MOI of approximately 0.2 using media supplemented with 8 $\mu\text{g}/\text{mL}$ polybrene (EMD Millipore). Cells expressing EGFP were enriched by FACS and single-cell clonal lines were derived.

Generation of knockout cell lines using CRISPR-Cas9

Heterogeneous knockout cell populations were generated using lentiCRISPR v2 (Addgene #52961) or lentiCRISPR-hygro. lentiCRISPR-Hygro was constructed by replacing the puromycin resistance ORF in lentiCRISPR v2 with a hygromycin resistance ORF. A silent mutation was introduced into a BsmBI restriction site within the hygromycin resistance ORF to prevent fragmentation of the vector when cloning sgRNA oligos. sgRNA sequences (Appendix, Table 5) were cloned as described previously (6). An sgRNA targeting an irrelevant gene (*PP1D*) or a non-targeting guide were used as negative controls.

To generate active lentivirus, 6×10^5 293T cells were first seeded in 6-well dishes and transfected the following day using a 5:3:2 ratio of lentiCRISPR:psPAX2 (Addgene #12260):pMD2.G (Addgene #12259) using FuGENE HD and 1 μ g of total plasmid per well. Media were changed the next day. Two days after transfection, media were collected and passed through a 0.45 μ m SFCA sterile filter. Media containing the virus were diluted 1:1 with fresh media and used to transduce recipient cells overnight in a final polybrene concentration of 8 μ g/mL. Media were changed 24 hours later, and cells were split into fresh media containing 1 μ g/mL puromycin 48 hours after transduction.

To generate clonal knockout lines, single-cell cloning was performed after infection with lentiCRISPR v2, lentiCRISPR-hygro, or after transient transfection of PX330 (Addgene #42230) targeting the gene of interest.

Transfection with miR-19 inhibitors

3×10^5 reporter cells were seeded per well in six-well dishes. Cells were transfected the following day with a mixture of inhibitors for miR-19a and miR-19b at 5 nM each (MiRIDIAN microRNA Hairpin Inhibitors, GE Dharmacon) using Lipofectamine RNAiMAX (Thermo Fisher). Fluorescence was assessed by flow cytometry 48 hours after transfection.

Genome-wide CRISPR-Cas9 screening

Lentiviral sgRNA library production

The human GeCKO v2 library was obtained from Addgene (#1000000048) and amplified according to the provided instructions. Plasmid was purified from bacterial pellets using the Qiagen plasmid maxi kit. Active lentivirus was prepared in 293T cells by first seeding 3.2×10^6 cells per 10 cm dish. GeCKO library A and library B were prepared independently using 15 dishes per library. The day after seeding, each dish was transfected using 10 μ g of total plasmid (5:3:2 ratio of GeCKO library:psPAX2:pMD2.G), 30 μ L of FuGENE HD, and 900 μ L of Opti-MEM. Media was exchanged the following day. Media collections at 48 and 72 hours after transfection were pooled prior to filtering through a 0.45 μ m SFCA sterile filter. Aliquots of the library were snap frozen on dry ice and ethanol before being stored at -80°C . Library titer was determined as described (6).

Transduction of reporter cell lines with lentiCRISPR library

Replicate genome-wide CRISPR-Cas9 screens using HCT116^{EGFP-miR-19}, HCT116^{EGFP}, or ANKRD52^{-/-} HCT116^{EGFP-miR-19} cells were performed for lentiCRISPR libraries A and B. For each transduction, five 12-well plates were seeded with 5×10^5 reporter cells per well. An overnight transduction was performed the following day by diluting virus to an MOI of 0.2-0.4 in 8 $\mu\text{g/mL}$ polybrene. Cells were then trypsinized and pooled before being plated into fresh medium in six 15 cm dishes. 48 hours later, cells were trypsinized, pooled, counted, and seeded into five 15 cm dishes with 1 $\mu\text{g/mL}$ puromycin using 2.4×10^7 cells per dish. In parallel, a small aliquot of cells was used to confirm that an MOI of 0.2-0.4 was achieved. Cells were passaged for 12-14 days before sorting. At every passage, 1×10^7 cells were seeded per dish into four 15 cm dishes with medium containing puromycin. At least 2×10^7 cells were transduced with each library for each screen, corresponding to ~300X or greater coverage.

Cell sorting

Two days prior to sorting, ten 15 cm dishes with 1.2×10^7 cells per dish were seeded for each library-reporter pair. Samples were prepared for FACS by trypsinization in 0.25% trypsin-EDTA (Thermo Fisher) for 7 minutes. Cells were dissociated by pipetting up and down approximately 20 times with a P1000 pipet to minimize doublets. Dissociated cells were pipetted directly into media, pelleted at 300 g for 5 minutes, and washed once with PBS. Cells were resuspended at 1.4×10^7 cells per mL in PBS supplemented with 3% FBS. Cells were sorted at the UT Southwestern Flow Cytometry Core Facility

using a MoFlo cell sorter (Beckman Coulter). The brightest or dimmest 0.5% of cells were collected based on EGFP fluorescence. Cell sorting was performed on approximately 9×10^7 cells, and typical yields ranged from 2×10^5 – 3×10^5 sorted bright/dim cells. Cells were pelleted at 300 g and frozen at -80°C for genomic DNA (gDNA) extraction. Unsorted cells were similarly collected.

Genomic DNA extraction

gDNA was extracted from the unsorted cells using the Qiagen DNeasy Blood & Tissue Kit according to the manufacturer's instructions. Extractions were performed on 4×10^7 cells using 5×10^6 cells per column to ensure enough gDNA for 300X coverage of the library. DNA was eluted by adding 125 μL of water to each column. The same eluate was added back to the column for a second elution. The DNA concentration in the final eluate was assessed using the Qubit dsDNA BR assay kit (Thermo Fisher).

To facilitate maximum recovery of gDNA from the sorted cells, a previously described method (115) was used with the following modifications: Sorted cell pellets were resuspended in 500 μL of tissue lysis buffer, consisting of 460 μL of STE buffer [1 mM EDTA (pH 8.0), 10 mM Tris-HCl (pH 8.0), 100 mM NaCl] supplemented with 10 μL of 0.5 M EDTA, 10 μL of proteinase K [10 mg/mL in TE buffer containing 10 mM Tris-HCl (pH 8.0) and 1 mM EDTA], and 20 μL of 10% SDS. Pellets were digested overnight at 55°C while shaking at 1000 rpm on a Thermomixer (Eppendorf). The following day, 5 μL of 2 mg/mL RNase A was added to each tube and incubated at 37°C for 1 hr while shaking at 1000 rpm. Extractions were performed with an equal volume of pH 7.9-

buffer saturated phenol, followed by phenol:chloroform:isoamyl alcohol (25:24:1), followed by chloroform. 20 µg of glycogen (Roche) and 1.5 mL of 100% ethanol was added to each tube and DNA was precipitated at -80°C for 1 hr followed by centrifugation at 18,000 g for 10 min at 4°C. Pellets were washed with 1 mL of 75% ethanol, dried, and resuspended in 21 µL of water by incubating at 37°C for a minimum of 4 hrs. DNA concentration was determined with the Qubit dsDNA BR assay kit.

Sequencing library preparation

Methods to prepare PCR amplicon libraries for deep sequencing were adapted from a previously published protocol (6). All primer sequences are provided in Appendix, Table 5. For unsorted cells, an initial round of PCR (PCR I) was performed using 6.6 µg of gDNA per 100 µL PCR reaction. To maintain 300X coverage, 20 reactions were assembled for each sample. For sorted cells, all extracted gDNA for a given sample was distributed into two 100 µL reactions. In both cases, 18 cycles of amplification were performed using Herculase II Fusion polymerase (Agilent). All reactions for a given sample from PCR I were then pooled together and a second round of PCR (PCR II) was performed to add the necessary adapters for Illumina sequencing. Due to variable PCR efficiency between samples, the cycle number for PCR II was adjusted so that each library was amplified in a 50 µL reaction to a common endpoint with respect to DNA quantity (approximately 50 ng of DNA library in a 50 µL PCR sample).

DNA was purified for sequencing using AMPure XP beads (Agencourt) according to the manufacturer's instructions with the following modifications: Each 50 µL PCR II reaction

was mixed with 25 μ L of beads and incubated for 5 minutes. Magnetic separation was used to collect the supernatant. The supernatant was mixed with 90 μ L of beads and incubated for 5 minutes. The supernatant was collected and discarded. Beads were washed twice with 200 μ L of 70% ethanol and then dried for approximately 12 minutes. Bound DNA was eluted from the beads using 40 μ L of water.

Next-generation sequencing

Prior to sequencing, all DNA libraries were analyzed using the Bioanalyzer High Sensitivity DNA Analysis Kit (Agilent). Library concentration was then determined by qPCR using the KAPA Library Quantification Kit for Illumina platforms. All samples were sequenced on an Illumina HiSeq 2500 or a NextSeq 500 with 75 bp single reads. ~15-20 million reads were sequenced per library.

Sequencing data analysis

A reference file for all sgRNAs in the library was acquired from Addgene, and identical sgRNAs targeting more than one protein-coding gene were removed. Demultiplexed FASTQ files were mapped to the reference file using Bowtie 2 requiring unique alignments with no mismatches. Normalized read counts were calculated as described previously (6). Screen hits were identified using RIGER (83) with the following parameters: log fold-change ranking, 1×10^6 permutations, second best rank (SBR) scoring algorithm.

qRT-PCR

RNA was extracted from cells using the miRNeasy Mini Kit (Qiagen) with an on-column DNase digestion. cDNA was generated using either the SuperScript IV First-Strand Synthesis System (Thermo Fisher) or MultiScribe Reverse Transcriptase (Thermo Fisher). SYBR Green assays were performed using the SYBR Green PCR Master Mix (Applied Biosystems) using primer pairs listed in Appendix, Table 5. TaqMan assays for mature miRNAs were performed using pre-designed assays (catalog numbers provided in Appendix, Table 5 and the TaqMan Universal Master Mix II (Applied Biosystems). A custom Taqman assay was designed for pri-miR-17-92 (sequences provided in Appendix, Table 5).

RNA-seq

Wild-type, *AGO2*^{-/-}, and *ANKRD52*^{-/-} HCT116^{EGFP-miR-19} cells were used for RNA-seq. Three independent clonal *AGO2*^{-/-} and *ANKRD52*^{-/-} knockout cell lines and 3 biological triplicates of wild-type cells were sequenced. 5.0x10⁵ cells were seeded per well in six-well dishes. Cells were harvested 48 hours later, and RNA was extracted using the RNeasy Mini Kit (Qiagen) with an on-column DNase digestion. Sequencing libraries were generated using the TruSeq Stranded mRNA LT Sample Prep Kit (Illumina) and run on a NextSeq 500 using the NextSeq 500/550 High Output v2 Kit, 75 cycle (Illumina). Data were analyzed as reported previously (116) with updated versions of edgeR (v3.8.6) and Cufflinks (v2.2.1).

Co-immunoprecipitation assays

For all co-IP assays, 3.2×10^6 293T cells were seeded one day before transfection. Cells were transfected using Fugene HD with 10 μg of total plasmid. Media were changed the following day. Cells were harvested 48 hours after transfection. Cells were washed once, scraped in PBS, and lysed on ice for 10 minutes in 1 mL of lysis buffer composed of 25 mM Tris-HCl (pH 8.0), 150 mM NaCl, 2 mM MgCl_2 , 0.5% NP-40, 1 mM DTT, and a protease inhibitor cocktail (cOmplete EDTA-free, Roche). Lysates were spun at 10,000 g for 10 minutes. Supernatants were collected and diluted with 0.5 volumes of fresh lysis buffer. 1.5 μL of IP antibody [anti-V5 (Invitrogen Cat# 46-0705) or anti-HA (Cell Signaling Cat# 2367S)] was added to each sample and rotated at 4°C for 30 minutes. 30 μL of washed Dynabeads Protein G (Thermo Fisher) were added to each sample and incubated for 6 hours. RNase A (Thermo Fisher) was added to a final concentration of 20 $\mu\text{g}/\text{mL}$ where indicated. Samples were washed four times in ice-cold lysis buffer. 50 μL of 2X Laemmli sample buffer were added to each sample and aliquots were used for western blot analysis.

Western blot antibodies

Antibodies used for western blotting included anti-HA (2367S, Cell Signaling), anti-V5 (46-0705, Invitrogen), anti-AGO2 (SAB4200085, Sigma), anti-GAPDH (2118S, Cell Signaling), anti-alpha-Tubulin (T6199-200UL, Sigma), anti-BRD4 (13440S, Cell Signaling), anti-CTNNB1 (9587S, Cell Signaling), anti-POU2F1 (8157S, Cell Signaling), anti-ANKRD52 (A302-372A, Bethyl), and anti-CSNK1A1 (sc-6477, Santa Cruz).

Phos-tag SDS-PAGE electrophoresis

SDS-PAGE gels with 7% acrylamide were supplemented with Phos-tag AAL solution (Wako) according to manufacturer's recommendations. Gels were run at 100V in an XCELL SureLOCK Mini-Cell (Invitrogen) until the dye front completely exited the gel. Gels were incubated in transfer buffer supplemented with 1 mM EDTA for 10 minutes. Gels were then soaked in normal transfer buffer for 10 minutes. Proteins were transferred to a nitrocellulose membrane and standard western blotting procedures were subsequently followed.

For lambda phosphatase treatments, lysates were generated as described in the co-immunoprecipitation assays. 50 μ L of lysate was mixed with 10X $MnCl_2$ buffer and 10X reaction buffer provided with the lambda protein phosphatase kit (NEB). Samples treated with enzyme received 1 μ L of purified lambda protein phosphatase. Incubations were performed for 45 minutes at 30°C, and samples were subjected to chloroform-methanol precipitation (117) prior to phos-tag electrophoresis.

Mass spectrometry

Endogenous AGO2 was purified from *ANKRD52*^{+/+} and *ANKRD52*^{-/-} HCT116 cells. *AGO2*^{-/-} cells were used as a control. 1×10^7 cells were seeded per 15 cm dish, and eight dishes were used per cell line. AGO2 was immunoprecipitated using methods

adapted from an established protocol (118) with 100 μ L of Dynabeads Protein G loaded with 18 μ g of anti-AGO2 antibody (SAB4200085, Sigma) per purification. IP eluates were resuspended in 5x Laemmli sample buffer.

FH-AGO2 constructs (WT, T830A, S824A/T830A) were stably expressed using MSCV-puro in *ANKRD52*^{-/-} cells. 1×10^7 cells were seeded per 15 cm dish, and eight dishes were used per cell line. Media were changed 48 hours later. Cells were scraped in PBS 72 hours after plating. Lysates were generated using methods similar to the co-immunoprecipitation assays, with the exception that a phosphatase inhibitor cocktail (PhosStop, Roche) was included and lysate supernatants were diluted with one volume of lysis buffer. Proteins were immunoprecipitated using 100 μ L of Dynabeads Protein G loaded with 20 μ g of anti-FLAG antibody (F1804, Sigma). Beads were rotated at 4°C for 3 hours. Beads were washed five times in lysis buffer. Proteins were eluted using 70 μ L of 2x Laemmli sample buffer per 100 μ L of beads.

Purified AGO2 proteins were separated by SDS-PAGE and stained using InstantBlue (Expedeon). Gel slices containing AGO2 bands were reduced by DTT, alkylated by iodoacetic acid, and digested with trypsin (Trypsin Gold; Promega). The digestion was stopped by adding formic acid, followed by peptide extraction in acetonitrile. Extracted peptides were desalted by C18 ZipTip (Millipore).

Peptide mixtures were separated by C-18 resin (100 Å, 3 μ m, MICHROM Bioresources) in-house packed into a silica capillary emitter (100 μ m ID, 100 mm resin length). LC gradient was generated by a Dionex Ultimate 3000 nanoLC system (Thermo Scientific), using mobile phase A: 0.1% formic acid and B: 0.1% formic acid in acetonitrile. Mobile phase gradient: 2% B at 0-15 min, 30% B at 81 min, 35% B at 85 min, 40% B at 87 min,

60% B at 95 min, 80% B at 96-107 min and 2% B at 108-120 min. Flow rate: 600 nL/min at 0-13.5 min, 250 nL/min at 13.5-120 min.

Peptide eluents were sprayed online with a nano-electrospray ion source (Thermo Scientific) at spray voltage of 1.5 kV and capillary temperature of 250° C. High resolution MS analysis was performed on a QExactive Quadrupole-Orbitrap Hybrid mass spectrometer (Thermo Scientific), which operates in data-dependent mode with dynamic exclusion of 30s. Full scan MS was acquired at the m/z range of 300-1650, resolution of 70,000 and automatic gain control (AGC) target of $3e6$. The top 15 most intense ions were subsequently selected for HCD fragmentation at resolution of 17,500, collision energy of 27 and AGC target of $1e5$.

Proteome data analysis was performed using Mascot (Matrix Science) and Proteome Discoverer (1.4, Thermo Scientific). The raw data were searched against the human proteome database (Uniprot, UP000005640) plus common contaminants. Static modification was cysteine carbamidomethylation; variable modifications were serine or threonine phosphorylation, methionine oxidation and glutamine or asparagine deamination. Precursor mass tolerance was 20 ppm and fragment mass tolerance, 0.05 Da. Maximum number of miscleavage sites allowed was 2. After peptide identification, precursor ion intensities were quantified manually in XCalibur using extracted ion chromatogram.

Cloning, mutagenesis, and expression of cDNA constructs

Sequences of all primers used for cloning are provided in Appendix, Table 5. FLAG-HA-AGO2 (FH-AGO2) was PCR amplified from pIRES-neo-FLAG/HA AGO2 (Addgene #10822) and subcloned into pcDNA3.1+. FH-AGO2 mutants were generated using the QuikChange II XL Site-Directed Mutagenesis Kit (Agilent) or by cloning customized gBlocks (IDT) into the parental pcDNA3.1+ vector containing FH-AGO2 (sequence of all mutants provided in Appendix, Table 5). For stable expression of wild-type or mutant FH-AGO2, constructs were subcloned into pMSCV-puro (Clontech). FLAG-HA-AGO1 was subcloned from pIRESneo-FLAG/HA AGO1 (Addgene #10820) into pMSCV-PIG (Addgene #21654). V5-tagged ANKRD52 (corresponding to NP_775866.2) was constructed by PCR amplification from HCT116 cDNA followed by cloning into pcDNA3.1+. cDNA clones for human PPP6C and CSNK1A1 were obtained from the Invitrogen Ultimate ORF LITE Library (Clone ID #IOH7224 and IOH59150, respectively) and subcloned into pCAGIG (Addgene #11159) using Gateway LR Clonase (Thermo Fisher). For tethering assays, a 5X BoxB sequence adapted from a previous report (95) was designed as a gBlock (IDT) and cloned in the XbaI site of pGL3-Control (Promega) (sequence in Appendix, Table 5). For the λ N constructs, a gBlock containing the λ N peptide sequence with an HA tag (95) was subcloned into pcDNA3.1-FH-AGO2, replacing the FLAG-HA tag. To generate control plasmid expressing λ N-HA peptide alone, the λ N-HA sequence was PCR amplified and cloned into pcDNA3.1+.

AGO2:miRNA and AGO2:mRNA association studies

For experiments involving endogenous AGO2, parental HCT116 cells were used. For analysis of FH-AGO2 miRNA or mRNA binding, cells stably expressing the indicated wild-type or mutant FH-AGO2 protein were first generated by infecting *AGO2*^{-/-} HCT116 cells with MSCV retroviruses. Then, for each IP sample, 6×10^6 cells were seeded per 10 cm dish. Cells were harvested 48 hours later by scraping in PBS. Pelleted cells were resuspended in 1 mL of a lysis buffer consisting of 25 mM Tris-HCl (pH 8.0), 150 mM NaCl, 2 mM MgCl₂, 0.5% NP-40, 1 mM DTT, a protease inhibitor cocktail (cOmplete, EDTA-free, Roche), and 250 U/mL Recombinant RNasin Ribonuclease Inhibitor (Promega). Cells were lysed on ice for 10 minutes. Samples were spun at 10,000 g for 10 minutes. Supernatant fractions were retained. Protein concentration was determined using the Bio-Rad DC Protein Assay Kit, and all samples were adjusted to the same concentration with lysis buffer. Dynabeads Protein G (Thermo Fisher) were prepared by pre-incubating with 1.5 µg of antibody [either anti-FLAG (F1804, Sigma) or anti-AGO2 (SAB4200085, Sigma)] and pre-blocking with 0.5 mg/mL BSA, 0.5 mg/mL yeast tRNA, and 0.2 mg/mL heparin. Each sample was incubated with 25 µL of prepared Dynabeads Protein G for 3 hours at 4°C. Samples were washed three times in lysis buffer. Captured protein was eluted from the beads using either 2.5 mg/mL 3X FLAG peptide (Sigma) or 3.5 mg/mL AGO2 peptide [sequence derived from (118), synthesized at the UT Southwestern Protein Chemistry Technology Core] dissolved in lysis buffer. 80% of the eluate was harvested for RNA extraction and 20% was diluted with 2x Laemmli sample buffer for western blot analysis. For each IP, qRT-PCR assays were performed to determine input and IP levels for mature miRNAs and mRNA targets of interest. Western blot analysis was performed to determine the relative amount of

AGO2 in the IP eluate. RNA quantity as a percent of input was determined for all IP eluates and then normalized to the relative amount of protein captured in each eluate.

AGO2 capture using an mRNA target mimic

Experiments to capture AGO2 loaded with miRNA were adapted from a previously published method(93). *ANKRD52*^{+/+} and *ANKRD52*^{-/-} HCT116^{EGFP-miR-19} cells were seeded at 1.35×10^7 cells per dish in six 15 cm dishes per cell line. 48 hours later, cells from each dish were scraped in PBS, pelleted, and lysed on ice for 10 minutes in 1 mL of a buffer containing 25 mM Tris-HCl (pH 8.0), 150 mM NaCl, 2 mM MgCl₂, 0.5% NP-40, 1 mM DTT, a protease inhibitor cocktail (cOmplete, EDTA-free, Roche), a phosphatase inhibitor cocktail (PhosStop, Roche), and 250 U/mL Recombinant RNasin Ribonuclease Inhibitor (Promega). Lysates were spun at 10,000 g for 10 minutes and supernatants were further diluted with one volume of lysis buffer. To assess binding of AGO2 to the target mimic, 1.8 mL of each lysate was incubated with 50 μ L of washed Dynabeads MyOne Streptavidin C1 (Thermo Fisher) pre-loaded with 300 pmol of wild type or mutant RNA oligonucleotide (Appendix, Table 5) and pre-blocked with 1 mg/mL BSA, 0.5 mg/mL yeast tRNA, and 0.2 mg/mL heparin. To assess AGO2 phosphorylation after immunoprecipitation, 1.8 mL of each lysate was incubated with 50 μ L of washed Dynabeads Protein G (Thermo Fisher) pre-incubated with 5 μ L of anti-AGO2 antibody [SAB4200085, Sigma (118)] and pre-blocked as noted previously. Lysates were incubated with beads for 3 hours at room temperature. Beads were washed four times in lysis buffer before 50 μ L of 2X Laemmli sample buffer was added.

Phos-tag electrophoresis was performed on captured protein complexes and on input protein samples subjected to chloroform-methanol precipitation (117).

Tethering assays

293T cells were seeded in 24-well plates using 7.5×10^4 cells per well. Cells were transfected the following day using FuGENE HD and 301 ng of total plasmid. Each transfection consisted of 1 ng of phRL-SV40 (Promega), 20 ng of pGL3-Control or pGL3-BoxB, 150 ng of pcDNA3.1+ (expressing tethered or untethered proteins), and 130 ng of empty pcDNA3.1+. Cells were harvested 24 hours later for luciferase activity assays using the Dual-Luciferase Reporter Assay System (Promega). Firefly luciferase activity was normalized to *Renilla* luciferase activity in each well to control for variation in transfection efficiency. Biological triplicates were performed for each transfection.

Rapamycin treatment of reporter cells

ANKRD52^{-/-} HCT116^{EGFP-miR-19} cells were seeded in 6-well dishes at 6×10^5 cells per well. The following day, cells were treated with 10, 50, or 200 nM rapamycin for 72 hours (fresh media with rapamycin was exchanged at 48 hours). Cells were harvested in 2X Laemmli sample buffer at the experimental endpoint.

In vitro kinase assays using immunopurified FLAG-HA-AGO2

AGO2^{-/-} cells were infected with MSCV retroviral constructs to stably express wild-type FH-AGO2 or 5xA FH-AGO2. FH-AGO2-expressing cells were seeded using 1.5x10⁷ cells per dish in 15 cm dishes with three dishes per cell line. Lysates were generated using methods similar to the co-immunoprecipitation assays, with the exception that 2 mL of lysis buffer was used per dish. Lysates were diluted with one volume of lysis buffer. FH-AGO2 was immunoprecipitated using 9 µg of anti-FLAG antibody (F1804, Sigma) and 150 µL of washed Dynabeads. Samples were rotated at 4°C overnight. Beads were washed three times with lysis buffer and then treated with lambda protein phosphatase (NEB) for 45 minutes. Beads were washed three times with lysis buffer and then resuspended in 100 µL reaction buffer composed of 25 mM Tris-HCl (pH 7.5), 10 mM MgCl₂, 2.5 mM DTT, 0.01% Triton X-100, 0.5 mg/mL BSA, 0.5 mM EGTA, 0.5 mM Na₃VO₄, 5 mM beta-glycerophosphate, 170 ng of recombinant CSNK1A1 (PV3850, Thermo Fisher), and 200 µM [γ -³²P]ATP (SA = 100-500 cpm/pmol). Reactions were incubated at 37°C for 2 hrs. Beads were separated and mixed with 50 µL of 2X Laemmli sample buffer. SDS-PAGE was performed, and gels were stained using SimplyBlue SafeStain (Invitrogen). ³²P signal was detected using a phosphor screen (GE Healthcare) and Typhoon FLA 7000 (GE Healthcare).

In vitro kinase assays using AGO2 peptides

In vitro CSNK1A1 kinase assays were performed using assay conditions adapted from manufacturer recommendations (Recombinant CSNK1A1, PV3850, Thermo Fisher). All reactions were performed in a 50 µL volume for 90 minutes at 30°C. Assay buffer was

composed of 25 mM Tris-HCl (pH 7.5), 10 mM MgCl₂, 2.5 mM DTT, 0.01% Triton X-100, 0.5 mg/mL BSA, 0.5 mM EGTA, 0.5 mM Na₃VO₄, 5 mM beta-glycerophosphate, 1 mM peptide (Appendix, Table 5), 170 ng of recombinant CSNK1A1, and 200 μM [γ -³²P]ATP (SA = 100-500 cpm/pmol). Reactions were terminated using 75 mM H₃PO₄ and spotted onto P81 phosphocellulose squares. Samples were washed four times in 75 mM H₃PO₄ for 5 minutes per wash and immersed in acetone for 5 minutes before drying. ³²P incorporation was assessed by Cerenkov counting.

APPENDIX

Table 1: Simulated sgRNA enrichment in the top 0.5% brightest cells.

	sgRNA fold enrichment (sorted / unsorted)				
Magnitude derepression (% of DROSHA)	100% guide efficacy	80% guide efficacy	60% guide efficacy	40% guide efficacy	20% guide efficacy
100	189.62	151.84	113.62	76.54	38.62
80	156.66	126.82	93.7	63.82	31.8
60	97.68	79.6	57.9	39.18	20.14
40	38.8	30.88	23.32	16.22	8.76
20	8.48	7.4	5.74	4.54	2.84
<p>*NOTE: Magnitude derepression is represented as the percentage of the maximum possible derepression of the EGFP reporter, assuming DROSHA knockout results in complete miRNA loss of function. Guide efficacy indicates percentage of cells infected with a given sgRNA-expressing lentivirus that acquire a null phenotype.</p>					

Table 2: Top 50 genes by RIGER analysis of CRISPR-Cas9 screen in HCT116^{EGFP-miR19} cells.

Gene	NES	Gene rank	p-value	p-value rank
ANKRD52	0.0000653 7	1	0.00000 1	1
XRN1	0.0002288	2	0.00000 1	2
hsa-mir-19b-1	0.0005649	3	0.00000 2	5
PPP6C	0.0006047	4	0.00000 2	6
DROSHA	0.0008498	5	0.00000 2	3
DDX6	0.001062	6	0.00000 2	4
DICER1	0.001389	7	0.00000 3	7
POU2F1	0.001536	8	0.00000 5	8
CTNNB1	0.001716	9	0.00000 6	9
XPO5	0.001749	10	0.00000 6	10

DGCR8	0.002239	11	0.00001 1	11
PRSS42	0.004118	12	0.00004 6	12
BMP1	0.004347	13	0.00004 8	13
BRD4	0.004805	14	0.00006 9	14
ARHGAP15	0.005981	15	0.00012 8	15
PPEF1	0.006569	16	0.00017	16
AGO2	0.006602	17	0.00017	17
TMEM234	0.007354	18	0.00021 1	19
ZFX	0.007403	19	0.00021 4	20
SLC16A6	0.008171	20	0.00026	21
TGM5	0.00871	21	0.00029 9	23
P2RY12	0.008776	22	0.00030 4	24
GPR135	0.008825	23	0.00030 8	25

OSMR	0.009021	24	0.00031 9	26
C19orf82	0.009211	25	0.00020 6	18
TAF7	0.009266	26	0.00033 7	27
C2orf72	0.009429	27	0.00034 2	28
TLX2	0.00956	28	0.00035	29
TGIF1	0.01016	29	0.00038 8	31
hsa-mir-1306	0.01227	30	0.00035 4	30
CDH3	0.0152	31	0.00088 5	34
RBP3	0.01585	32	0.00094 9	35
MAGEB4	0.01616	33	0.00099 4	36
CYP27A1	0.01652	34	0.00103 8	37
TMEM102	0.01781	35	0.00118 9	39

CLN5	0.01788	36	0.00119 8	40
EGLN3	0.01809	37	0.00123 3	41
CREB5	0.01868	38	0.00131 3	42
NonTargetingControlGuideForHuman_ 0262	0.01892	39	0.00029	22
FAT1	0.01938	40	0.00143 7	43
GK2	0.01986	41	0.00150 3	44
KMT2D	0.01995	42	0.00080 1	33
hsa-mir-92a-1	0.01997	43	0.00105 1	38
CNOT2	0.02064	44	0.00162 3	47
FGFR1	0.0209	45	0.00166 9	48
GPR83	0.02118	46	0.00171 2	49

RPS6KA5	0.02128	47	0.00173 2	50
ZNF641	0.02162	48	0.00178 4	51
DIXDC1	0.0217	49	0.0018	52
UPK2	0.02172	50	0.00180 1	53

Table 3: Top 50 genes by RIGER analysis of CRISPR-Cas9 screen in HCT116^{EGFP} cells.

Gene	NES	Gene rank	p-value	p-value rank
STK40	0.002925	1	0.000019	1
AQP12B	0.005491	2	0.000098	2
IRS1	0.008449	3	0.000279	3
YTHDC1	0.009152	4	0.000331	4
ZC3H15	0.009789	5	0.000365	5
ST8SIA2	0.01041	6	0.000409	6
PLEKHA2	0.01074	7	0.000433	7
PPP1R9A	0.01119	8	0.000475	8
RPL27	0.01126	9	0.000484	9
FLRT3	0.0118	10	0.000535	10
ANGPT1	0.01208	11	0.000558	11
RGS17	0.01229	12	0.000581	12
NKX3-2	0.0124	13	0.000593	13
IL20RB	0.01317	14	0.000679	14
RS1	0.01343	15	0.000698	15
NEIL3	0.01347	16	0.0007	16
NIPSNAP1	0.01399	17	0.000756	17
CLEC3A	0.01425	18	0.000786	18
C2orf88	0.01441	19	0.000809	19

QRICH1	0.01456	20	0.000819	20
TRMT61B	0.01466	21	0.000825	21
NCOA5	0.01616	22	0.000994	22
TMOD3	0.01626	23	0.001007	23
SMAD9	0.01636	24	0.001019	24
MIER2	0.017	25	0.00109	25
TMPRSS11A	0.01783	26	0.00119	27
SOX4	0.01793	27	0.001209	28
MMP7	0.01811	28	0.001235	29
RBBP9	0.01816	29	0.00124	30
ANK3	0.01891	30	0.001351	32
PAK3	0.01901	31	0.001363	33
BDH2	0.01907	32	0.001376	34
SMIM21	0.01928	33	0.001418	35
RFX3	0.01958	34	0.001474	36
VSIG1	0.01979	35	0.001497	37
KIF14	0.02026	36	0.001572	38
NUP37	0.02043	37	0.001591	39
AADAT	0.02064	38	0.001623	40
EAPP	0.02089	39	0.001667	41
LOC554223	0.0209	40	0.001669	42
FAM110B	0.02164	41	0.001786	44
KLHL28	0.02169	42	0.001797	45

MRPL50	0.02178	43	0.001815	46
ZNF605	0.02257	44	0.001936	47
RPS6KA5	0.02314	45	0.002047	48
ATP9A	0.02345	46	0.002098	49
CELF2	0.02419	47	0.002231	50
C5orf54	0.02432	48	0.002252	51
C4BPB	0.02468	49	0.002304	52
IPO5	0.02473	50	0.002318	53

Table 4: Top 50 genes by RIGER analysis of CRISPR-Cas9 screen in *ANKRD52*^{-/-} HCT116^{EGFP-miR19} cells.

Gene	NES	Gene rank	p-value	p-value rank
PRDM4	0.00003268	1	0.000001	1
LATS2	0.00008171	2	0.000001	4
CELF1	0.0001634	3	0.000001	2
IGF2BP3	0.0005066	4	0.000001	3
MBNL1	0.0009478	5	0.000002	5
CSNK1A1	0.001454	6	0.000003	6
NF2	0.002811	7	0.000017	7
EP300	0.00286	8	0.000018	8
COL6A3	0.002909	9	0.000019	9
MGME1	0.003219	10	0.000023	10
MRGBP	0.00335	11	0.000024	11
APMAP	0.003791	12	0.000039	12
FKBPL	0.004086	13	0.000044	13
MGA	0.005736	14	0.000114	14
CSDE1	0.006161	15	0.00014	15
CASP10	0.008449	16	0.000279	16
VSX1	0.008825	17	0.000308	17
SDCBP2	0.009723	18	0.000361	18
RBBP9	0.01002	19	0.000376	20

KEAP1	0.01128	20	0.000485	23
JAK3	0.01134	21	0.000492	24
SNX5	0.01167	22	0.000519	25
CST9L	0.01208	23	0.000558	26
YAE1D1	0.01245	24	0.0006	28
EIF3H	0.01275	25	0.000628	29
TH	0.01322	26	0.000682	30
STRAP	0.01347	27	0.0007	31
VPS39	0.0135	28	0.000703	32
TMEM144	0.01361	29	0.000714	33
SLC52A3	0.01369	30	0.000723	34
hsa-mir-5000	0.01371	31	0.000439	21
ZCCHC17	0.01422	32	0.000784	35
NRD1	0.01446	33	0.00081	36
RIT2	0.01474	34	0.000838	38
CALCA	0.01499	35	0.000863	39
HIST1H2BA	0.015	36	0.000864	40
NKX2-4	0.01512	37	0.000877	41
TCTA	0.0158	38	0.000943	42
HMHB1	0.01628	39	0.000832	37
SEMA3D	0.01654	40	0.001039	44
FAR2	0.01667	41	0.001052	45
TMEM74B	0.01727	42	0.001124	46

C1orf54	0.0174	43	0.001142	47
TCL1B	0.01753	44	0.001167	48
CMTR2	0.01776	45	0.001002	43
GNB2L1	0.01838	46	0.001275	49
ENTPD6	0.01868	47	0.001313	50
EIF4G1	0.01892	48	0.001354	53
C16orf71	0.01907	49	0.001376	54
SRSF6	0.01956	50	0.001469	56

Table 5: Oligonucleotide and peptide sequences.

<u>Generati</u> <u>on of</u> <u>MSCV</u> <u>Reporte</u> <u>rs</u>		
Primer name	Description	Sequence (5' to 3')
EGFP_ Fwd_Bg III	Forward primer to amplify EGFP	CTGAGAGATCTACCATGGTGAGCAAGG
EGFP_ Rev_Xh ol	Reverse primer to amplify EGFP	CTGAGCTCGAGTTACTTGTACAGCTCGTCCATG
gBlock name	Description	Sequence (5' to 3')
miR- 19_Imp erfect	gBlock with 8x miR-19 binding sites cloned into MSCV-EGFP	GAATTCCTGGTTAACGACGGGTCCCTCAGTTTTGCCCTATTTGCACAA ATTTGAGTTTTGCCCTATTTGCACAGGGTCCCTCAGTTTTGCCCTATTT GCACAAATTTGAGTTTTGCCCTATTTGCACAGGGTCCCTCAGTTTTGCC CTATTTGCACAAATTTGAGTTTTGCCCTATTTGCACAGGGTCCCTCAGT TTTTGCCCTATTTGCACAAATTTGAGTTTTGCCCTATTTGCACAGGGTCC CGACGTTTAAACGACATCGAT
		*Bold lettering indicates miR-19 binding sites.

<u>Cloning</u> <u>lentiCRI</u> <u>SPR-</u> <u>Hygro</u>		
Primer name	Description	Sequence (5' to 3')
Lcv2_Hygro_Fwd	Generate PCR product with hygro cassette (forward)	CTGAGGGATCCGGCGCAACAACTTCTCTCTGCTGAAACAAGCCGGA GATGTCTGAAGAGAATCCTGGACCGATGAAAAAGCCTGAACTCAC
Lcv2_Hygro_Rev	Generate PCR product with hygro cassette (reverse)	CTGAGTGTACACGGTCGGCATCTACTCTAT
Lc_Hygro_Mut_F	Subclone hygro fragment with mutant BsmBI site (forward)	ACCGCGACGTCTGTCTGAGAAAGTTTCTGATCGAAAAGTTTCGACAGCGTG TCCGACCTGATGCAGCTCTCGGAGGGCGAAGAATCTCGTGCTTTC
Lc_Hygro_Mut_R	Subclone hygro fragment with mutant BsmBI site (reverse)	CCAGAGGTTGATTGTCTGACTT

<u>Oligonucleotides used to generate knockout cell lines</u>		
Primer name	Description	Sequence (5' to 3')
DROSH A-1F	sgRNA sequence targeting DROSHA (forward)	caccgGGGAGACTGTGATCCGGTAG
DROSH A-1R	sgRNA sequence targeting DROSHA (reverse)	aaacCTACCGGATCACAGTCTCCCc
EGFP1-1F	sgRNA sequence targeting EGFP (forward)	caccgGGGCGAGGAGCTGTTACCG
EGFP1-1R	sgRNA sequence targeting EGFP (reverse)	aaacCGGTGAACAGCTCCTCGCCCc
PPID-1F	sgRNA sequence	caccgAAAGGCATTGGACACACGAC

	targeting PPID (forward)	
PPID- 1R	sgRNA sequence targeting PPID (reverse)	aaacGTCGTGTGTCCAATGCCTTc
human_ Non- Target- 1F	sgRNA sequence, non-targeting (forward)	caccgATCGTTTCCGCTTAACGGCG
human_ Non- Target- 1R	sgRNA sequence, non-targeting (reverse)	aaacCGCCGTTAAGCGGAAACGATc
AGO2- 1F	sgRNA sequence targeting AGO2 (forward)	caccgTAACGCCTGCAAGCTCACGC
AGO2- 1R	sgRNA sequence targeting AGO2 (reverse)	aaacGCGTGAGCTTGCAGGCGTTAc
ANKRD 52-1F	sgRNA sequence	caccgCCTGTTGAGCAGCCTCAACG

	targeting ANKRD52 (forward)	
ANKRD 52-1R	sgRNA sequence targeting ANKRD52 (reverse)	aaacCGTTGAGGCTGCTCAACAGGc
ANKRD 52-2F	sgRNA sequence targeting ANKRD52 (forward)	caccgGCGTTCCTACTCTCGCAGA
ANKRD 52-2R	sgRNA sequence targeting ANKRD52 (reverse)	aaacTCTGCGAGAGTAGGGAACGCc
PPP6C- 1F	sgRNA sequence targeting PPP6C (forward)	caccgCAGTTCTGAACAGTTCACAA
PPP6C- 1R	sgRNA sequence targeting PPP6C (reverse)	aaacTTGTGAACTGTTCAGAACTGc

PPP6C- 2F	sgRNA sequence targeting PPP6C (forward)	caccgTCAACACCAGTAACAGTGTG
PPP6C- 2R	sgRNA sequence targeting PPP6C (reverse)	aaacCACACTGTTACTGGTGTGAc
BRD4_F 1	sgRNA sequence targeting BRD4 (forward)	caccgTAAGATCATTAAAACGCCTA
BRD4_ R1	sgRNA sequence targeting BRD4 (reverse)	aaacTAGGCGTTTTAATGATCTTAc
BRD4_F 2	sgRNA sequence targeting BRD4 (forward)	caccgGTCGATGCTTGAGTTGTGTT
BRD4_ R2	sgRNA sequence targeting	aaacAACACAACCTCAAGCATCGACc

	BRD4 (reverse)	
CTNNB 1_F1	sgRNA sequence targeting CTNNB1 (forward)	caccgAGAACGCATGATAGCGTGTC
CTNNB 1_R1	sgRNA sequence targeting CTNNB1 (reverse)	aaacGACACGCTATCATGCGTTCTc
CTNNB 1_F2	sgRNA sequence targeting CTNNB1 (forward)	caccgAATGCAGTTCGCCTTCACTA
CTNNB 1_R2	sgRNA sequence targeting CTNNB1 (reverse)	aaacTAGTGAAGGCGAACTGCATTc
POU2F 1_F1	sgRNA sequence targeting POU2F1 (forward)	caccgAGGAGCAATCTCAACAGCCC

POU2F 1_R1	sgRNA sequence targeting POU2F1 (reverse)	aaacGGGCTGTTGAGATTGCTCCTc
POU2F 1_F2	sgRNA sequence targeting POU2F1 (forward)	caccgGTTGAGATTGCTCCTCCTAC
POU2F 1_R2	sgRNA sequence targeting POU2F1 (reverse)	aaacGTAGGAGGAGCAATCTCAACc
mTOR_ 1F	sgRNA sequence targeting mTOR (forward)	caccgCCAGCTCAGATGCCAATGAG
mTOR_ 1R	sgRNA sequence targeting mTOR (reverse)	aaacCTCATTGGCATCTGAGCTGGc
mTOR_ 2F	sgRNA sequence targeting	caccgGCTCCAGCACTATGTCACCA

	mTOR (forward)	
mTOR_ 2R	sgRNA sequence targeting mTOR (reverse)	aaacTGGTGACATAGTGCTGGAGCc
CSNK1 A1_1F	sgRNA sequence targeting CSNK1A1 (forward)	caccgTGACTTATGTTAGCTGACC
CSNK1 A1_1R	sgRNA sequence targeting CSNK1A1 (reverse)	aaacGGTCAGCTAACATAAGTACAc
CSNK1 A1_2F	sgRNA sequence targeting CSNK1A1 (forward)	caccgTTTACCTTTAGCCCTTGCCA
CSNK1 A1_2R	sgRNA sequence targeting CSNK1A1 (reverse)	aaacTGGCAAGGGCTAAAGGTAAAc

LATS2- 1F	sgRNA sequence targeting LATS2 (forward)	caccgTCCAAACTACATCGCACCCG
LATS2- 1R	sgRNA sequence targeting LATS2 (reverse)	aaacCGGGTGCGATGTAGTTTGGAc
LATS2- 2F	sgRNA sequence targeting LATS2 (forward)	caccgGATGTGTCTAACTGTCCGGTG
LATS2- 2R	sgRNA sequence targeting LATS2 (reverse)	aaacCACCGACAGTTAGACACATCc
SRPK1_ 1F	sgRNA sequence targeting SRPK1 (forward)	caccgATAATACCCCTGCTGACATT
SRPK1_ 1R	sgRNA sequence targeting	aaacAATGTCAGCAGGGGTATTATc

	SRPK1 (reverse)	
SRPK1_ 2F	sgRNA sequence targeting SRPK1 (forward)	caccgAGATCTGAAACTCAGCACCG
SRPK1_ 2R	sgRNA sequence targeting SRPK1 (reverse)	aaacCGGTGCTGAGTTTCAGATCTc
		*Lowercase letters denote sequences added for cloning
<u>Oligonucleotides used</u> <u>for CRISPR-Cas9</u> <u>Screening</u>		
Primer name	Description	Sequence (5' to 3')
Gecko_ F1	PCR I Forward Primer	AATGGACTATCATATGCTTACCGTAACTTGAAAGTATTTTCG
Gecko_ R1	PCR I Reverse Primer	TCTACTATTCTTTCCCCTGCACTGTgtgggggatgtgcgctctg
Gecko_ F2_A	PCR II Forward Primer A	AATGATACGGCGACCACCGAGATCTACACTCTTTCCCTACACGACGCT CTTCCGATCTtAAGTAGAGtcttgtggaaaggacgaaacaccg

Gecko_ F2_B	PCR II Forward Primer B	AATGATACGGCGACCACCGAGATCTACACTCTTTCCCTACACGACGCT CTTCCGATCTatACACGATCtcttgaggaaaggacgaaacaccg
Gecko_ F2_C	PCR II Forward Primer C	AATGATACGGCGACCACCGAGATCTACACTCTTTCCCTACACGACGCT CTTCCGATCTgatCGCGCGGTtcttgaggaaaggacgaaacaccg
Gecko_ F2_D	PCR II Forward Primer D	AATGATACGGCGACCACCGAGATCTACACTCTTTCCCTACACGACGCT CTTCCGATCTcgatCATGATCGtcttgaggaaaggacgaaacaccg
Gecko_ F2_E	PCR II Forward Primer E	AATGATACGGCGACCACCGAGATCTACACTCTTTCCCTACACGACGCT CTTCCGATCTtcgatCGTTACCActcttgaggaaaggacgaaacaccg
Gecko_ F2_F	PCR II Forward Primer F	AATGATACGGCGACCACCGAGATCTACACTCTTTCCCTACACGACGCT CTTCCGATCTatcgatTCCTTGGTtcttgaggaaaggacgaaacaccg
Gecko_ F2_G	PCR II Forward Primer G	AATGATACGGCGACCACCGAGATCTACACTCTTTCCCTACACGACGCT CTTCCGATCTgatcgatAACGCATTtcttgaggaaaggacgaaacaccg
Gecko_ F2_H	PCR II Forward Primer H	AATGATACGGCGACCACCGAGATCTACACTCTTTCCCTACACGACGCT CTTCCGATCTcgatcgatACAGGTATtcttgaggaaaggacgaaacaccg
Gecko_ F2_I	PCR II Forward Primer I	AATGATACGGCGACCACCGAGATCTACACTCTTTCCCTACACGACGCT CTTCCGATCTacgatcgatAGGTAAGGtcttgaggaaaggacgaaacaccg
Gecko_ F2_J	PCR II Forward Primer J	AATGATACGGCGACCACCGAGATCTACACTCTTTCCCTACACGACGCT CTTCCGATCTtACAATGGtcttgaggaaaggacgaaacaccg

Gecko_ F2_K	PCR II Forward Primer K	AATGATACGGCGACCACCGAGATCTACACTCTTTCCCTACACGACGCT CTTCCGATCTatACTGTATCtcttgaggaaaggacgaaacaccg
Gecko_ F2_L	PCR II Forward Primer L	AATGATACGGCGACCACCGAGATCTACACTCTTTCCCTACACGACGCT CTTCCGATCTgatAGGTGCGAtcttgaggaaaggacgaaacaccg
Gecko_ F2_M	PCR II Forward Primer M	AATGATACGGCGACCACCGAGATCTACACTCTTTCCCTACACGACGCT CTTCCGATCTcgatACGACAGAtcttgaggaaaggacgaaacaccg
Gecko_ F2_N	PCR II Forward Primer N	AATGATACGGCGACCACCGAGATCTACACTCTTTCCCTACACGACGCT CTTCCGATCTtcgatACACTGTGtcttgaggaaaggacgaaacaccg
Gecko_ F2_O	PCR II Forward Primer O	AATGATACGGCGACCACCGAGATCTACACTCTTTCCCTACACGACGCT CTTCCGATCTatcgatGACACGACtcttgaggaaaggacgaaacaccg
Gecko_ F2_P	PCR II Forward Primer P	AATGATACGGCGACCACCGAGATCTACACTCTTTCCCTACACGACGCT CTTCCGATCTgatcgatACTCGATGtcttgaggaaaggacgaaacaccg
Gecko_ F2_Q	PCR II Forward Primer Q	AATGATACGGCGACCACCGAGATCTACACTCTTTCCCTACACGACGCT CTTCCGATCTcgatcgatGTGATAGCtcttgaggaaaggacgaaacaccg
Gecko_ F2_R	PCR II Forward Primer R	AATGATACGGCGACCACCGAGATCTACACTCTTTCCCTACACGACGCT CTTCCGATCTacgatcgatGAGACACTtcttgaggaaaggacgaaacaccg
Gecko_ F2_S	PCR II Forward Primer S	AATGATACGGCGACCACCGAGATCTACACTCTTTCCCTACACGACGCT CTTCCGATCTaACTCAGAGtcttgaggaaaggacgaaacaccg

Gecko_ F2_T	PCR II Forward Primer T	AATGATACGGCGACCACCGAGATCTACACTCTTTCCCTACACGACGCT CTTCCGATCTtaCACTCGTAtcttgaggaaaggacgaaacaccg
Gecko_ F2_U	PCR II Forward Primer U	AATGATACGGCGACCACCGAGATCTACACTCTTTCCCTACACGACGCT CTTCCGATCTctaGACATACAtcttgaggaaaggacgaaacaccg
Gecko_ F2_V	PCR II Forward Primer V	AATGATACGGCGACCACCGAGATCTACACTCTTTCCCTACACGACGCT CTTCCGATCTgctaCACACAGAtcttgaggaaaggacgaaacaccg
Gecko_ F2_W	PCR II Forward Primer W	AATGATACGGCGACCACCGAGATCTACACTCTTTCCCTACACGACGCT CTTCCGATCTagctaTACACTCActtgaggaaaggacgaaacaccg
Gecko_ F2_X	PCR II Forward Primer X	AATGATACGGCGACCACCGAGATCTACACTCTTTCCCTACACGACGCT CTTCCGATCTtagctaTCAGCTATcttgaggaaaggacgaaacaccg
Gecko_ R2	PCR II Reverse Primer	CAAGCAGAAGACGGCATAACGAGATGTGACTGGAGTTCAGACGTGTGC TCTTCCGATCTtctactattcttcccctgcactgt
<u>TaqMan</u> <u>Assays</u> for <u>miRNAs</u>		
miRNA assayed	Catalog number (Thermo Fisher)	Assay Numer

miR-19a	4427975	000395
miR-19b	4427975	000396
miR-92a	4427975	000430
let-7b	4427975	000378
let-7d	4427975	002283
miR-16	4427975	000391
miR-21	4427975	000397
miR-26a	4427975	000405
<u>Primers</u>		
for <u>SYBR</u> <u>Green</u> <u>qRT-</u> <u>PCR</u> <u>assays</u>		
Primer name	Description	Sequence (5' to 3')
CCNE1 _SYBR_ F	CCNE1 Forward Primer	ggccaaaatcgacaggac
CCNE1 _SYBR_ R	CCNE1 Reverse Primer	gggtctgcacagactgcat
EGFP_ SYBR_2 _F	EGFP Forward Primer	cctgaagttcatctgcacca

EGFP_ SYBR_2 _R	EGFP Reverse Primer	ggtcagggtggtcacgag
HMGA2 _SYBR_ F	HMGA2 Forward Primer	tccctctaaagcagctcaaaa
HMGA2 _SYBR_ R	HMGA2 Reverse Primer	acttggtggccattcct
MYC_S YBR_F	MYC Forward Primer	CACCACCAGCAGCGACTCT
MYC_S YBR_R	MYC Reverse Primer	CTTTTCCACAGAAACAACATCGAT
<u>Custom</u> <u>TaqMan</u> <u>assay</u> <u>for pri-</u> <u>miR-17-</u> <u>92</u>		
Oligonu cleotide name	Description	Sequence (5' to 3')
Hsa_17- 92_F	pri-miR-17- 92 primer (forward)	GGCCAGCCGAAGATGGT

Hsa_17-92_R	pri-miR-17-92 primer (reverse)	GCAGTTAGGTCCACGTGTATGACA
Hsa_17-92_Probe	TaqMan probe	CGGCTACTCCTCC
<u>Cloning</u> <u>ANKRD</u> <u>52 from</u> <u>cDNA</u>		
Primer name	Description	Sequence (5' to 3')
ANKRD52_5'_fragment_F	Primers used to amplify 5' part of ANKRD52 from cDNA (forward)	CTGAGGCTAGCCCTCAGCATCACGGACCA
ANKRD52_5'_fragment_R	Primers used to amplify 5' part of ANKRD52 from cDNA (reverse)	GCACATGCTCATTGCTGAGT
ANKRD52_3'_fragment	Primers used to amplify 3' part of	ACATGTTCCCCCTGCACTTA

agment _F	ANKRD52 from cDNA (forward)	
ANKRD 52_3'_fr agment _R	Primers used to amplify 3' part of ANKRD52 from cDNA (reverse)	CTGAGGAATTCCACCCAGTCGTGTTCTCCTT
<u>AGO2</u> <u>Mutant</u> <u>Sequen</u> <u>ces</u>		
Mutant name	AGO2 DNA sequence (5' to 3', region D823 - N835 of AGO2)	
WT	GACAGTGC TGAAGGAA GCCATACC TCTGGGCA GAGTAAC	
5xA	GACGCTGC TGAAGGAG CCCATGCC	

	GCTGGGCA GGCTAAC	
5xE	GACGAGGC TGAAGGAG AGCATGAG GAGGGGCA GGAGAAC	
S824A	GACGCTGC TGAAGGAA GCCATACC TCTGGGCA GAGTAAC	
S828A	GACAGTGC TGAAGGAG CCCATACC TCTGGGCA GAGTAAC	
T830A	GACAGTGC TGAAGGAA GCCATGCC TCTGGGCA GAGTAAC	
S831A	GACAGTGC TGAAGGAA GCCATACC GCTGGGCA GAGTAAC	

S834A	GACAGTGC TGAAGGAA GCCATACC TCTGGGCA GGCTAAC	
S824A/ T830A	GACGCTGC TGAAGGAA GCCATGCC TCTGGGCA GAGTAAC	
S824E	GACGAGGC TGAAGGAA GCCATACC TCTGGGCA GAGTAAC	
S828E	GACAGTGC TGAAGGAG AGCATACC TCTGGGCA GAGTAAC	
T830E	GACAGTGC TGAAGGAA GCCATGAG TCTGGGCA GAGTAAC	
S831E	GACAGTGC TGAAGGAA GCCATACC	

	GAGGGGCA GAGTAAC	
S834E	GACAGTGC TGAAGGAA GCCATACC TCTGGGCA GGAGAAC	
S824E/ S828E	GACGAGGC TGAAGGAG AGCATACC TCTGGGCA GAGTAAC	
S824E/ S831E	GACGAGGC TGAAGGAA GCCATACC GAGGGGCA GAGTAAC	
S828E/ S831E	GACAGTGC TGAAGGAG AGCATACC GAGGGGCA GAGTAAC	
S824E/ S828E/ S831E	GACGAGGC TGAAGGAG AGCATACC GAGGGGCA GAGTAAC	

<u>Generating constructs for tethering assays</u>		
Primer name	Description	Sequence (5' to 3')
LNHA_F	Primers to amplify the lambda N HA peptide (forward)	CCAAGCTGGCTAGCGTTTA
LNHA_R	Primers to amplify the lambda N HA peptide (reverse)	CTCAGGAATTCTTAGCCGCTAGCGTAATCGGGCACG
gBlock name	Description	Sequence (5' to 3')
5X_Box B	5X BoxB insert cloned into pGL3-Control	CTGAGTCTAGATTCCCTAAGTCCAACACTAACTGGGGATTCCCTGGG CCCTGAAGAAGGGCCCCTCGACTAAGTCCAACACTAACTGGGCCCT GAAGAAGGGCCCATATAGGGCCCTGAAGAAGGGCCCTATCGAGGATA TTATCTCGACTAAGTCCAACACTAACTGGGCCCTGAAGAAGGGCCC ATATAGGGCCCTGAAGAAGGGCCCTATCGAGGATATTATCTCGAGTCT AGACTGAG

LNHA_AGO2_Fragment	LNHA_AGO2 fragment cloned into pcDNA3.1-AGO2 (WT and 5xE)	CTGAGGGATCCACTAGTCCAGTGTGGTGGGAATTCACCATGGACGCAC AAACACGACGACGTGAGCGTCGCGCTGAGAAACAAGCTCAATGGAAA GCTGCAAACCCACCGCTCGAGGCTGCCCAAGCTTACACCATGGCCTA CCCTTATGACGTGCCCGATTACGCTAGCGGCCGCATGTACTIONCGGGAG CCGGCCCCGCACTTGACCTCCTGCGCCGCCGCCCCCATCCAAGGA TATGCCTTCAAGCCTCCACCTAGACCCGACTTTGGGACCTCCGGGAGA ACAATCAAATTACAGGCCAATTTCTTCGAAATGGACATCCCCAAAATTG ACATCTATCATTATGAATTGGATATCAAGCCAGAGAAGTGCCCGAGGA GAGTTAACCTGAG
<u>RNA oligonucleotides used to capture AGO2:miR-21</u>		
Oligonucleotide name	Description	Sequence (5' to 3')
WT_miR-21_Capture_Oligo	5' biotin modification, 2'-O-methylated throughout (WT)	GAUGAACCACUCAGAGACAU AAGCUAAUCUA
Mutant_miR-21_Capture_Oligo	5' biotin modification, 2'-O-methylated throughout (Mutant)	GAUGAACCACAGUCAGACUAUUCGAUAUCUA

<u>Peptides used for <i>in vitro</i> kinase assays</u>		
Peptide name	Description	Peptide sequence
WT	Wild-type AGO2 sequence	D-K-E-H-D-S-A-E-G-S-H-T-S-G-Q-S-N-G-R-D-R
5xA	5xA AGO2 sequence	D-K-E-H-D-A-A-E-G-A-H-A-A-G-Q-A-N-G-R-D-R
pS824	Phosphoserine at S824	D-K-E-H-D-pS-A-E-G-S-H-T-S-G-Q-S-N-G-R-D-R
pS828	Phosphoserine at S828	D-K-E-H-D-S-A-E-G-pS-H-T-S-G-Q-S-N-G-R-D-R
pS824_S828	Phosphoserine at S824, S828 intact, 3XA	D-K-E-H-D-pS-A-E-G-S-H-A-A-G-Q-A-N-G-R-D-R
pS828_T830	Phosphoserine at S828, T830 intact, 3XA	D-K-E-H-D-A-A-E-G-pS-H-T-A-G-Q-A-N-G-R-D-R
pS828_S831	Phosphoserine at S828,	D-K-E-H-D-A-A-E-G-pS-H-A-S-G-Q-A-N-G-R-D-R

	S831 intact, 3XA	
pS831_ S834	Phosphoserine at S831, S834 intact, 3XA	D-K-E-H-D-A-A-E-G-A-H-A-pS-G-Q-S-N-G-R-D-R

BIBLIOGRAPHY

1. D. P. Bartel, MicroRNAs: target recognition and regulatory functions. *Cell* **136**, 215-233 (2009).
2. E. F. Finnegan, A. E. Pasquinelli, MicroRNA biogenesis: regulating the regulators. *Crit Rev Biochem Mol Biol* **48**, 51-68 (2013).
3. I. Heo, V. N. Kim, Regulating the regulators: posttranslational modifications of RNA silencing factors. *Cell* **139**, 28-31 (2009).
4. J. T. Mendell, E. N. Olson, MicroRNAs in stress signaling and human disease. *Cell* **148**, 1172-1187 (2012).
5. N. E. Sanjana, O. Shalem, F. Zhang, Improved vectors and genome-wide libraries for CRISPR screening. *Nat Methods* **11**, 783-784 (2014).
6. O. Shalem *et al.*, Genome-scale CRISPR-Cas9 knockout screening in human cells. *Science* **343**, 84-87 (2014).
7. F. Crick, Central dogma of molecular biology. *Nature* **227**, 561-563 (1970).
8. T. R. Cech, J. A. Steitz, The noncoding RNA revolution-trashing old rules to forge new ones. *Cell* **157**, 77-94 (2014).
9. R. Schweet, R. Heintz, Protein synthesis. *Annu Rev Biochem* **35**, 723-758 (1966).
10. N. A. Faustino, T. A. Cooper, Pre-mRNA splicing and human disease. *Genes Dev* **17**, 419-437 (2003).
11. I. Ulitsky, D. P. Bartel, lincRNAs: genomics, evolution, and mechanisms. *Cell* **154**, 26-46 (2013).
12. R. C. Lee, R. L. Feinbaum, V. Ambros, The *C. elegans* heterochronic gene *lin-4* encodes small RNAs with antisense complementarity to *lin-14*. *Cell* **75**, 843-854 (1993).
13. B. Wightman, I. Ha, G. Ruvkun, Posttranscriptional regulation of the heterochronic gene *lin-14* by *lin-4* mediates temporal pattern formation in *C. elegans*. *Cell* **75**, 855-862 (1993).
14. B. J. Reinhart *et al.*, The 21-nucleotide *let-7* RNA regulates developmental timing in *Caenorhabditis elegans*. *Nature* **403**, 901-906 (2000).
15. M. Lagos-Quintana, R. Rauhut, W. Lendeckel, T. Tuschl, Identification of novel genes coding for small expressed RNAs. *Science* **294**, 853-858 (2001).
16. N. C. Lau, L. P. Lim, E. G. Weinstein, D. P. Bartel, An abundant class of tiny RNAs with probable regulatory roles in *Caenorhabditis elegans*. *Science* **294**, 858-862 (2001).
17. R. C. Lee, V. Ambros, An extensive class of small RNAs in *Caenorhabditis elegans*. *Science* **294**, 862-864 (2001).
18. G. Hutvagner *et al.*, A cellular function for the RNA-interference enzyme Dicer in the maturation of the *let-7* small temporal RNA. *Science* **293**, 834-838 (2001).
19. A. Grishok *et al.*, Genes and mechanisms related to RNA interference regulate expression of the small temporal RNAs that control *C. elegans* developmental timing. *Cell* **106**, 23-34 (2001).
20. Y. Lee, K. Jeon, J. T. Lee, S. Kim, V. N. Kim, MicroRNA maturation: stepwise processing and subcellular localization. *EMBO J* **21**, 4663-4670 (2002).
21. Y. Lee *et al.*, The nuclear RNase III Drosha initiates microRNA processing. *Nature* **425**, 415-419 (2003).
22. Z. Mourelatos *et al.*, miRNPs: a novel class of ribonucleoproteins containing numerous microRNAs. *Genes Dev* **16**, 720-728 (2002).
23. R. I. Gregory, T. P. Chendrimada, N. Cooch, R. Shiekhattar, Human RISC couples microRNA biogenesis and posttranscriptional gene silencing. *Cell* **123**, 631-640 (2005).
24. R. S. Pillai *et al.*, Inhibition of translational initiation by *Let-7* MicroRNA in human cells. *Science* **309**, 1573-1576 (2005).

25. P. H. Olsen, V. Ambros, The lin-4 regulatory RNA controls developmental timing in *Caenorhabditis elegans* by blocking LIN-14 protein synthesis after the initiation of translation. *Dev Biol* **216**, 671-680 (1999).
26. C. P. Petersen, M. E. Bordeleau, J. Pelletier, P. A. Sharp, Short RNAs repress translation after initiation in mammalian cells. *Mol Cell* **21**, 533-542 (2006).
27. L. P. Lim *et al.*, Microarray analysis shows that some microRNAs downregulate large numbers of target mRNAs. *Nature* **433**, 769-773 (2005).
28. J. Krutzfeldt *et al.*, Silencing of microRNAs in vivo with 'antagomirs'. *Nature* **438**, 685-689 (2005).
29. H. Guo, N. T. Ingolia, J. S. Weissman, D. P. Bartel, Mammalian microRNAs predominantly act to decrease target mRNA levels. *Nature* **466**, 835-840 (2010).
30. A. A. Bazzini, M. T. Lee, A. J. Giraldez, Ribosome profiling shows that miR-430 reduces translation before causing mRNA decay in zebrafish. *Science* **336**, 233-237 (2012).
31. S. Djuranovic, A. Nahvi, R. Green, miRNA-mediated gene silencing by translational repression followed by mRNA deadenylation and decay. *Science* **336**, 237-240 (2012).
32. S. W. Eichhorn *et al.*, mRNA destabilization is the dominant effect of mammalian microRNAs by the time substantial repression ensues. *Mol Cell* **56**, 104-115 (2014).
33. S. Bagga *et al.*, Regulation by let-7 and lin-4 miRNAs results in target mRNA degradation. *Cell* **122**, 553-563 (2005).
34. P. Landgraf *et al.*, A mammalian microRNA expression atlas based on small RNA library sequencing. *Cell* **129**, 1401-1414 (2007).
35. H. R. Chiang *et al.*, Mammalian microRNAs: experimental evaluation of novel and previously annotated genes. *Genes Dev* **24**, 992-1009 (2010).
36. R. C. Friedman, K. K. Farh, C. B. Burge, D. P. Bartel, Most mammalian mRNAs are conserved targets of microRNAs. *Genome Res* **19**, 92-105 (2009).
37. E. Bernstein *et al.*, Dicer is essential for mouse development. *Nat Genet* **35**, 215-217 (2003).
38. L. de Pontual *et al.*, Germline deletion of the miR-17 approximately 92 cluster causes skeletal and growth defects in humans. *Nat Genet* **43**, 1026-1030 (2011).
39. A. Ventura *et al.*, Targeted deletion reveals essential and overlapping functions of the miR-17 through 92 family of miRNA clusters. *Cell* **132**, 875-886 (2008).
40. C. L. Tan *et al.*, MicroRNA-128 governs neuronal excitability and motor behavior in mice. *Science* **342**, 1254-1258 (2013).
41. L. A. Medeiros *et al.*, Mir-290-295 deficiency in mice results in partially penetrant embryonic lethality and germ cell defects. *Proc Natl Acad Sci U S A* **108**, 14163-14168 (2011).
42. R. R. Chivukula *et al.*, An essential mesenchymal function for miR-143/145 in intestinal epithelial regeneration. *Cell* **157**, 1104-1116 (2014).
43. P. P. Medina, M. Nolde, F. J. Slack, OncomiR addiction in an in vivo model of microRNA-21-induced pre-B-cell lymphoma. *Nature* **467**, 86-90 (2010).
44. S. Costinean *et al.*, Pre-B cell proliferation and lymphoblastic leukemia/high-grade lymphoma in E(mu)-miR155 transgenic mice. *Proc Natl Acad Sci U S A* **103**, 7024-7029 (2006).
45. L. He *et al.*, A microRNA polycistron as a potential human oncogene. *Nature* **435**, 828-833 (2005).
46. P. Mu *et al.*, Genetic dissection of the miR-17~92 cluster of microRNAs in Myc-induced B-cell lymphomas. *Genes Dev* **23**, 2806-2811 (2009).
47. Y. C. Han *et al.*, An allelic series of miR-17~92-mutant mice uncovers functional specialization and cooperation among members of a microRNA polycistron. *Nat Genet* **47**, 766-775 (2015).
48. J. Kota *et al.*, Therapeutic microRNA delivery suppresses tumorigenesis in a murine liver cancer model. *Cell* **137**, 1005-1017 (2009).

49. K. A. O'Donnell, E. A. Wentzel, K. I. Zeller, C. V. Dang, J. T. Mendell, c-Myc-regulated microRNAs modulate E2F1 expression. *Nature* **435**, 839-843 (2005).
50. O. S. Rissland, S. J. Hong, D. P. Bartel, MicroRNA destabilization enables dynamic regulation of the miR-16 family in response to cell-cycle changes. *Mol Cell* **43**, 993-1004 (2011).
51. D. Gatfield *et al.*, Integration of microRNA miR-122 in hepatic circadian gene expression. *Genes Dev* **23**, 1313-1326 (2009).
52. T. C. Chang, M. Peretea, S. Lee, S. L. Salzberg, J. T. Mendell, Genome-wide annotation of microRNA primary transcript structures reveals novel regulatory mechanisms. *Genome Res* **25**, 1401-1409 (2015).
53. S. R. Viswanathan, G. Q. Daley, R. I. Gregory, Selective blockade of microRNA processing by Lin28. *Science* **320**, 97-100 (2008).
54. Y. Nam, C. Chen, R. I. Gregory, J. J. Chou, P. Sliz, Molecular basis for interaction of let-7 microRNAs with Lin28. *Cell* **147**, 1080-1091 (2011).
55. I. Heo *et al.*, Lin28 mediates the terminal uridylation of let-7 precursor MicroRNA. *Mol Cell* **32**, 276-284 (2008).
56. S. R. Viswanathan *et al.*, Lin28 promotes transformation and is associated with advanced human malignancies. *Nat Genet* **41**, 843-848 (2009).
57. H. I. Suzuki *et al.*, Modulation of microRNA processing by p53. *Nature* **460**, 529-533 (2009).
58. M. Mori *et al.*, Hippo signaling regulates microprocessor and links cell-density-dependent miRNA biogenesis to cancer. *Cell* **156**, 893-906 (2014).
59. Z. Paroo, X. Ye, S. Chen, Q. Liu, Phosphorylation of the human microRNA-generating complex mediates MAPK/Erk signaling. *Cell* **139**, 112-122 (2009).
60. J. Lopez-Orozco *et al.*, Functional analyses of phosphorylation events in human Argonaute 2. *RNA* **21**, 2030-2038 (2015).
61. H. H. Qi *et al.*, Prolyl 4-hydroxylation regulates Argonaute 2 stability. *Nature* **455**, 421-424 (2008).
62. K. M. Herbert, G. Pimienta, S. J. DeGregorio, A. Alexandrov, J. A. Steitz, Phosphorylation of DGCR8 increases its intracellular stability and induces a progrowth miRNA profile. *Cell Rep* **5**, 1070-1081 (2013).
63. J. Shen *et al.*, EGFR modulates microRNA maturation in response to hypoxia through phosphorylation of AGO2. *Nature* **497**, 383-387 (2013).
64. S. Rudel *et al.*, Phosphorylation of human Argonaute proteins affects small RNA binding. *Nucleic Acids Res* **39**, 2330-2343 (2011).
65. X. Tang, Y. Zhang, L. Tucker, B. Ramratnam, Phosphorylation of the RNase III enzyme Drosha at Serine300 or Serine302 is required for its nuclear localization. *Nucleic Acids Res* **38**, 6610-6619 (2010).
66. X. Tang, M. Li, L. Tucker, B. Ramratnam, Glycogen synthase kinase 3 beta (GSK3beta) phosphorylates the RNAase III enzyme Drosha at S300 and S302. *PLoS One* **6**, e20391 (2011).
67. D. H. Parry, J. Xu, G. Ruvkun, A whole-genome RNAi Screen for *C. elegans* miRNA pathway genes. *Curr Biol* **17**, 2013-2022 (2007).
68. R. Zhou *et al.*, Comparative analysis of argonaute-dependent small RNA pathways in *Drosophila*. *Mol Cell* **32**, 592-599 (2008).
69. M. Boutros, J. Ahringer, The art and design of genetic screens: RNA interference. *Nat Rev Genet* **9**, 554-566 (2008).
70. R. W. Carthew, E. J. Sontheimer, Origins and Mechanisms of miRNAs and siRNAs. *Cell* **136**, 642-655 (2009).
71. L. Cong *et al.*, Multiplex genome engineering using CRISPR/Cas systems. *Science* **339**, 819-823 (2013).

72. P. Mali *et al.*, RNA-guided human genome engineering via Cas9. *Science* **339**, 823-826 (2013).
73. M. Jinek *et al.*, RNA-programmed genome editing in human cells. *Elife* **2**, e00471 (2013).
74. T. Wang, J. J. Wei, D. M. Sabatini, E. S. Lander, Genetic screens in human cells using the CRISPR-Cas9 system. *Science* **343**, 80-84 (2014).
75. R. Barrangou *et al.*, Advances in CRISPR-Cas9 genome engineering: lessons learned from RNA interference. *Nucleic Acids Res* **43**, 3407-3419 (2015).
76. D. Kim *et al.*, Digenome-seq: genome-wide profiling of CRISPR-Cas9 off-target effects in human cells. *Nat Methods* **12**, 237-243, 231 p following 243 (2015).
77. O. Parnas *et al.*, A Genome-wide CRISPR Screen in Primary Immune Cells to Dissect Regulatory Networks. *Cell* **162**, 675-686 (2015).
78. J. Kluiver *et al.*, Rapid generation of microRNA sponges for microRNA inhibition. *PLoS One* **7**, e29275 (2012).
79. V. Olive *et al.*, miR-19 is a key oncogenic component of mir-17-92. *Genes Dev* **23**, 2839-2849 (2009).
80. Y. K. Kim, B. Kim, V. N. Kim, Re-evaluation of the roles of DROSHA, Exportin 5, and DICER in microRNA biogenesis. *Proc Natl Acad Sci U S A* **113**, E1881-1889 (2016).
81. T. Hart *et al.*, High-Resolution CRISPR Screens Reveal Fitness Genes and Genotype-Specific Cancer Liabilities. *Cell* **163**, 1515-1526 (2015).
82. P. V. Jallepalli *et al.*, Securin is required for chromosomal stability in human cells. *Cell* **105**, 445-457 (2001).
83. B. Luo *et al.*, Highly parallel identification of essential genes in cancer cells. *Proc Natl Acad Sci U S A* **105**, 20380-20385 (2008).
84. T. C. He *et al.*, Identification of c-MYC as a target of the APC pathway. *Science* **281**, 1509-1512 (1998).
85. J. Zuber *et al.*, RNAi screen identifies Brd4 as a therapeutic target in acute myeloid leukaemia. *Nature* **478**, 524-528 (2011).
86. B. Stefansson, T. Ohama, A. E. Daugherty, D. L. Brautigam, Protein phosphatase 6 regulatory subunits composed of ankyrin repeat domains. *Biochemistry* **47**, 1442-1451 (2008).
87. E. Kinoshita, E. Kinoshita-Kikuta, K. Takiyama, T. Koike, Phosphate-binding tag, a new tool to visualize phosphorylated proteins. *Mol Cell Proteomics* **5**, 749-757 (2006).
88. Y. Zeng, H. Sankala, X. Zhang, P. R. Graves, Phosphorylation of Argonaute 2 at serine-387 facilitates its localization to processing bodies. *Biochem J* **413**, 429-436 (2008).
89. N. T. Schirle, I. J. MacRae, The crystal structure of human Argonaute2. *Science* **336**, 1037-1040 (2012).
90. E. Elkayam *et al.*, The structure of human argonaute-2 in complex with miR-20a. *Cell* **150**, 100-110 (2012).
91. Q. Liu *et al.*, miR-16 family induces cell cycle arrest by regulating multiple cell cycle genes. *Nucleic Acids Res* **36**, 5391-5404 (2008).
92. C. Mayr, M. T. Hemann, D. P. Bartel, Disrupting the pairing between let-7 and Hmga2 enhances oncogenic transformation. *Science* **315**, 1576-1579 (2007).
93. C. F. Flores-Jasso, W. E. Salomon, P. D. Zamore, Rapid and specific purification of Argonaute-small RNA complexes from crude cell lysates. *RNA* **19**, 271-279 (2013).
94. J. M. Cummins *et al.*, The colorectal microRNAome. *Proc Natl Acad Sci U S A* **103**, 3687-3692 (2006).
95. R. S. Pillai, C. G. Artus, W. Filipowicz, Tethering of human Ago proteins to mRNA mimics the miRNA-mediated repression of protein synthesis. *RNA* **10**, 1518-1525 (2004).
96. U. Knippschild *et al.*, The casein kinase 1 family: participation in multiple cellular processes in eukaryotes. *Cell Signal* **17**, 675-689 (2005).

97. C. C. Wang, M. Tao, T. Wei, P. S. Low, Identification of the major casein kinase I phosphorylation sites on erythrocyte band 3. *Blood* **89**, 3019-3024 (1997).
98. J. Liu *et al.*, Argonaute2 is the catalytic engine of mammalian RNAi. *Science* **305**, 1437-1441 (2004).
99. J. A. Vidigal, A. Ventura, The biological functions of miRNAs: lessons from in vivo studies. *Trends Cell Biol* **25**, 137-147 (2015).
100. A. K. Leung *et al.*, Poly(ADP-ribose) regulates stress responses and microRNA activity in the cytoplasm. *Mol Cell* **42**, 489-499 (2011).
101. S. F. Wong *et al.*, Independent regulation of vertebral number and vertebral identity by microRNA-196 paralogs. *Proc Natl Acad Sci U S A* **112**, E4884-4893 (2015).
102. S. Miyaki *et al.*, MicroRNA-140 plays dual roles in both cartilage development and homeostasis. *Genes Dev* **24**, 1173-1185 (2010).
103. A. Ota *et al.*, Identification and characterization of a novel gene, C13orf25, as a target for 13q31-q32 amplification in malignant lymphoma. *Cancer Res* **64**, 3087-3095 (2004).
104. M. Ji *et al.*, The miR-17-92 microRNA cluster is regulated by multiple mechanisms in B-cell malignancies. *Am J Pathol* **179**, 1645-1656 (2011).
105. B. Schitteck, T. Sinnberg, Biological functions of casein kinase 1 isoforms and putative roles in tumorigenesis. *Mol Cancer* **13**, 231 (2014).
106. S. Konermann *et al.*, Genome-scale transcriptional activation by an engineered CRISPR-Cas9 complex. *Nature* **517**, 583-588 (2015).
107. K. Nakanishi, D. E. Weinberg, D. P. Bartel, D. J. Patel, Structure of yeast Argonaute with guide RNA. *Nature* **486**, 368-374 (2012).
108. H. Wang *et al.*, One-step generation of mice carrying mutations in multiple genes by CRISPR/Cas-mediated genome engineering. *Cell* **153**, 910-918 (2013).
109. E. Hodis *et al.*, A landscape of driver mutations in melanoma. *Cell* **150**, 251-263 (2012).
110. X. Bonilla *et al.*, Genomic analysis identifies new drivers and progression pathways in skin basal cell carcinoma. *Nat Genet* **48**, 398-406 (2016).
111. H. Kato *et al.*, Loss of protein phosphatase 6 in mouse keratinocytes increases susceptibility to ultraviolet-B-induced carcinogenesis. *Cancer Lett* **365**, 223-228 (2015).
112. K. Hayashi *et al.*, Abrogation of protein phosphatase 6 promotes skin carcinogenesis induced by DMBA. *Oncogene* **34**, 4647-4655 (2015).
113. S. Chen *et al.*, Genome-wide CRISPR screen in a mouse model of tumor growth and metastasis. *Cell* **160**, 1246-1260 (2015).
114. E. Elyada *et al.*, CK1alpha ablation highlights a critical role for p53 in invasiveness control. *Nature* **470**, 409-413 (2011).
115. D. A. Largaespada, L. S. Collier, Transposon-mediated mutagenesis in somatic cells: identification of transposon-genomic DNA junctions. *Methods Mol Biol* **435**, 95-108 (2008).
116. S. Lee *et al.*, Noncoding RNA NORAD Regulates Genomic Stability by Sequestering PUMILIO Proteins. *Cell* **164**, 69-80 (2016).
117. D. Wessel, U. I. Flugge, A method for the quantitative recovery of protein in dilute solution in the presence of detergents and lipids. *Anal Biochem* **138**, 141-143 (1984).
118. S. Rudel, A. Flatley, L. Weinmann, E. Kremmer, G. Meister, A multifunctional human Argonaute2-specific monoclonal antibody. *RNA* **14**, 1244-1253 (2008).